An Epigenetic Priming Mechanism Mediated by Nutrient Sensing Regulates Transcriptional Output during C. elegans Development

Natalia Stec, Katja Doerfel, Kelly Hills-Muckey, Victoria Ettorre, Sevinc Ercan, Wolfgang Keil, Christopher Hammell

An Epigenetic Priming Mechanism Mediated by Nutrient Sensing Regulates Transcriptional Output During *C. elegans* Development

Natalia Stec[1], Katja Doerfel[1], Kelly Hills-Muckey[1], Victoria M. Ettorre[2], Sevinc Ercan[2], Wolfgang Keil[3*], Christopher M. Hammell[1*]

[1]Cold Spring Harbor Laboratory, 1 Bungtown Road, Cold Spring Harbor, New York, 11724, USA
[2]New York University, Center for Genomics and Systems Biology, 100 Washington Square East, 852 Brown, New York, New York, 10003, USA
[3]Laboratoire Physico Chimie Curie, Institut Curie, PSL Research University, CNRS UMR168, 26 rue d'Ulm, 75248 Paris Cedex 05, France

*Correspondence: wolfgang.keil@curie.fr (W.K.), chammell@cshl.edu (C.M.H.)(lead contact)

Summary

While precise tuning of gene expression levels is critical for most developmental pathways, the mechanisms by which the transcriptional output of dosage-sensitive molecules is established or modulated by the environment remain poorly understood. Here, we provide a mechanistic framework for how the conserved transcription factor BLMP-1/Blimp1 operates as a pioneer factor to decompact chromatin near its target loci during embryogenesis (hours prior to major transcriptional activation) and by doing so, regulates both the duration and amplitude of subsequent target gene transcription during post-embryonic development. This priming mechanism is genetically separable from the mechanisms that establish the timing of transcriptional induction and functions to canalize aspects of cell-fate specification, animal size regulation, and molting. A key feature of the BLMP-1-dependent transcriptional priming mechanism is that chromatin decompaction is initially established during embryogenesis and maintained throughout larval development by nutrient sensing. This anticipatory mechanism integrates transcriptional output with environmental conditions and is essential for resuming normal temporal patterning after animals exit nutrient-mediated developmental arrests.

INTRODUCTION

Many developmental systems produce invariable phenotypes despite being confronted with perturbations, such as fluctuations in temperature and nutrient availability. How this robustness emerges from developmental gene regulatory networks (GRNs) and how aspects of precision and flexibility are balanced to generate robust developmental programs is a major open question in developmental biology. *C. elegans* serves as a unique genetic model for unraveling the mechanisms underlying precision and robustness of gene regulation during development. This is in part because the GRNs that control the essentially invariant cell lineage can generate the identical developmental outcomes in the context of diverse stochastic, environmental or genetic perturbations. A striking example of such a GRN is the so-called heterochronic pathway which controls the timing, sequence and synchrony of stage-specific patterns of cell divisions throughout post-embryonic development.[1] Analysis of this GRN indicates that it generates modular patterns of gene expression that occur in the context of the repetitive post-embryonic molting cycle which, in turn, demarcates the four successive larval stages (L1-L4). Transitions from one temporal program to the next occur through the expression of distinct microRNAs (miRNAs) that down-regulate the expression of their temporal selector gene targets in a strict dosage-sensitive manner. Ectopic or abnormally lower or higher doses of heterochronic genes (e.g. miRNAs) result in the wholesale skipping or reiteration of stage-specific developmental programs.[2-6] While the regulatory interactions that establish the sequence of stage-specific events are known, we have very little understanding of how the precise timing or levels of gene expression within this GRN are established and how both of these are buffered against perturbations to achieve robust temporal development of the animal.

High-temporal resolution transcriptomics studies have outlined a number of remarkable features associated with global gene expression patterns in developing *C. elegans* larva.[7,8] These studies indicate that between 10 to 20% of the post-embryonic transcriptome exhibits highly reproducible periodic expression patterns. Periodic transcription occurs in a variety of

environmental conditions and is independent of life history, indicating that it is under tight genetic control. Importantly, the transcriptional rhythm follows the cycle of post-embryonic molting, a process that demarcates patterns of stage-specific developmental programs. Under various environmental conditions that modulate overall developmental pace, the timing of transcription onset scales accordingly, such that the phase of transcription onset within the molting cycle is preserved.[7,8] Currently, it is not known how these transcriptional rhythms are generated, how they are integrated into the execution of stage-specific cellular programs, and how environmental or internal cues modulate features of these transcriptional patterns to achieve robust progression through developmental programs, even after prolonged developmental arrests.

The heterochronic GRN is integrated with global aspects of transcription as each of the miRNAs in this pathway exhibits an oscillatory expression. The most promising candidate gene that integrates the rhythm of *C. elegans* post-embryonic molting to changes in repetitive transcriptional patterns is *lin-42.* The *lin-42* gene encodes the *C. elegans* ortholog of PERIOD/Per proteins that are an essential component of the circadian clock in mice, *Drosophila* and humans.[9-11] Similar to PERIOD, LIN-42 functions as a transcriptional repressor and exhibits a cyclical expression pattern. In contrast to the temperature-invariant approximate 24-hour periodicity of *Period*, *lin-42* transcription is tied to the larval molting cycle, and thus, not temperature compensated.[5,11] Hypomorphic mutations in *lin-42* cause animals to prematurely execute adult-specific gene expression patterns in the L4 stage of larval development and these phenotypes are caused by the cumulative, premature over-expression of multiple heterochronic miRNAs.[5,6,12] In addition to these temporal patterning phenotypes, *lin-42* mutants also exhibit lengthened and irregular molting cycles.[11,13] The mechanisms by which LIN-42 negatively regulates heterochronic miRNA transcriptional output remain unknown. Furthermore, it is not known if other regulatory components exist that antagonize LIN-42 functions to ensure normal transcriptional regulation of developmental timing genes.

Here, we leverage the developmental phenotypes of *lin-42* mutations to identify BLMP-1 and ELT-3 as conserved transcription factors (TFs) that modulate the transcriptional output of many cyclically expressed genes to provide developmental robustness. We demonstrate that these TFs coordinate a plethora of post-embryonic developmental programs and we present a unique role for BLMP-1 in transcriptional priming that involves chromatin decompaction of target loci. Specifically, we show that BLMP-1 activity modulates the duration and amplitude of transcription of its targets without altering the timing of expression within the repetitive transcriptional cycle. We hypothesize that BLMP-1 functions specifically to assure proper transcriptional output in diverse environmental conditions. Consistent with this model, we demonstrate that the BLMP-1-dependent remodeling of chromatin is regulated by nutritional inputs and becomes essential when animals resume development after nutrient-mediated developmental arrests.

RESULTS

blmp-1 and *elt-3* Function in a partially redundant manner to control temporal patterning during larval development.

To identify genes that antagonize the function of LIN-42 to modulate transcriptional output, we took advantage of a highly penetrant phenotype of the *lin-42* loss of function allele *lin-42(n0189)* – the precocious expression of an adult-specific *col-19::GFP* reporter in both seam and syncytial hyp7 cells of the hypodermis (Figure 1A).[14] We used bacterial-mediated RNAi to deplete the expression of approximately 20 *C. elegans* candidate TFs in *lin-42(lf)* animals and then scored *col-19::GFP* expression in F_1 progeny. These transcription factors were selected based on known strong expression in the hypodermis[15] and/or previous implication in heterochronic developmental defects. The most reproducible suppressors of *lin-42* precocious phenotypes were bacterial RNAi clones expressing dsRNAs that target the *blmp-1* and *elt-3* loci (data not shown). We validated these findings with null alleles of these genes (*blmp-1(0)*

and *elt-3(0)*) which revealed a redundancy between *blmp-1* and *elt-3* that is distributed differentially across hypodermal cell types (Figure 1 A and B). Specifically, removal of *blmp-1* activity in *lin-42(lf)* mutants completely suppresses the precocious *col-19::GFP* expression in the lateral seam cells of L4-staged animals and only partially prevents early expression in hyp7 cells (Figure 1A and B). *lin-42(lf); elt-3(0)* mutants were only partially suppressed for the precocious *col-19::GFP* expression phenotypes. In contrast, combining *blmp-1(0)* and *elt-3(0)* mutations with *lin-42(lf)* mutations completely alleviated precocious *col-19::GFP* expression in both the seam and hyp7 cells of a majority of L4-staged animals (Figure 1A and B). This cell-type specific redundancy is likely due to the partially overlapping expression patterns of these TFs in hypodermal cells throughout larval development and indicate that BLMP-1 and ELT-3 are required for *lin-42(lf)* phenotypes (Figure 1C).[15]

Previous analysis of *blmp-1(0)* mutations indicate that BLMP-1 plays an important role in terminal fate specification of the hypodermis.[16] We sought to determine if *blmp-1* functions earlier in temporal cell fate specification when cells are proliferating. To this end, we assayed genetic interactions between *blmp-1* and *alg-1*, the latter encoding one of the two core miRISC argonaute components. *alg-1(0)* mutants ineffectively process most miRNAs (including heterochronic microRNAs) and exhibit relatively mild temporal patterning defects that resemble those associated with hypomorphic alleles of *let-7*.[17] To assay interactions, we quantified the number of seam cells at the mid L4 stage in wild-type or *alg-1(0)* mutant animals in conditions where we reduced *blmp-1* and/or *elt-3* activity using RNAi (Figure 1D, E). In wild-type animals, lateral seam cells exhibit highly reproducible cell division patterns that occur at specific stages of larval development (Figure 1F).[18] Defects in this lineage can be monitored by counting seam cell numbers in the L4 larval stage. Depletion of *elt-3* or *blmp-1* in wild-type animals resulted in the normal number of seam cells in the L4 stage. We observed a significant increase in the number of SCM::GFP(+) seam cells in *alg-1(0)*; *blmp-1* RNAi animals (Figure 1E). This expansion of lateral seam cell number could result from inappropriate reiteration of earlier, L2-

specific proliferative cell division programs, or conversion of normally asymmetric seam cell divisions in the L3 and L3-stage into symmetric ones (Figure 1F). Depletion of *blmp-1* in other mildly reiterative heterochronic mutants also resulted in similar enhancement of cell lineage and *col-19::GFP* expression phenotypes (Figure S1). *elt-3* RNAi did not significantly alter lateral seam cell numbers in *alg-1(0)* animals or enhance *alg-1(0); blmp-1(RNAi)* phenotypes. This indicates that BLMP-1 functions prior to terminal seam cell fate specification in larval development to control temporal cell fates in the hypodermis.

***blmp-1* and *elt-3* regulate diverse dosage-dependent developmental processes**

Development of *C. elegans* larva results in a fixed number of cells and a stereotypical size under standard growth conditions. Mutations in a number of pathways (including nutrient signaling, TGF-beta and MAP kinase pathways) or in structural components of the cuticle alter organismal size.[19] A shared feature of these regulatory and structural systems is that they function in a dose-sensitive manner wherein changes in the expression levels of individual elements within these pathways or components result in changes in animal morphology. As shown in Figure 2A, *blmp-1(0); elt-3(0)* animals exhibit a severe dumpy (*dpy)* phenotype. The *dpy* phenotype of *blmp-1(0); elt-3(0)* mutants manifests during post-embryonic development as freshly hatched *blmp-1(0); elt-3(0)* larvae are indistinguishable from wild-type animals (Figure 2A). *blmp-1(0)* single mutants exhibit less severe alterations in size and *elt-3(0)* animals are structurally normal (Figure 2A and B). These results demonstrate that in addition to modulating aspects of temporal cell-fate specification, *blmp-1* and *elt-3* cooperate to control animal morphology likely through the co-regulation of hypodermally expressed targets.

A majority of *blmp-1(0); elt-3(0)* animals precociously die two days after they reach adulthood due to the internal hatching of fertilized embryos (Figure 2C). Examination of dying *blmp-1(0); elt-3(0)* animals revealed that most are trapped in a partially shed cuticle (Figure 2D). Lethality is preceded by a reduction in movement and pharyngeal pumping approximately

8-10 hours after the L4-to-adult transition; a phenotype shared with other mutants that fail to post-transcriptionally down-regulate the adult expression of key genes involved in larval molting.[20] To determine if *blmp-1(0); elt-3(0)* animals inappropriately re-initiate molting programs during adulthood, we directly monitored the expression of a molting-specific GFP-pest transcriptional reporter, *mlt-10::GFP-pest*, in wild-type, single and double mutant animals. Wild type animals never expressed *mlt-10::GFP* as adults (n = 100) while a majority of *blmp-1(0); elt-3(0)* animals re-expressed the *mlt-10::GFP-pest* reporter (54%; n = 155) as adults (Figure 2E). *blmp-1(0)* single mutants also express *mlt-10::GFP-pest* within the same time period but with a much lower penetrance (18%, n = 137), consistent with previous observations using *blmp-1(RNAi)*.[21] These data indicate that *blmp-1* and *elt-3* function redundantly to halt the behavioral and physiological molting programs once animals transition into adulthood.

Development of the vulval structure in the L3 stage requires the integration of a number of interconnected signaling pathways that establish specific cell fates in vulval precursor cells (Figure 2F). One of the key initiating components in this process is *let-60*, encoding the *C. elegans* ortholog of the human Ras oncogene. Continued *let-60* activation commits vulval precursor cells (VPCs) to a 1° vulval cell fate specification pattern (Figure 2F). The induction of this fate specification is sensitive to the level of *let-60* activity.[22,23] For instance, the semi-dominant *let-60(n1046gf)* allele can induce ectopic vulval protrusions on the ventral surface (multi-vulva; *muv*) in 18% of animals harboring a single copy of this mutation (Figure 2G and H). We used this sensitized genetic context to determine whether *blmp-1(0)* and/or *elt-3(0)* mutations (or the combination of these mutations) leads to an elevation in VPC induction in *let-60(n1046)/+* animals. Lack of *blmp-1* activity significantly increased the penetrance and expressivity of the *muv* phenotype in *let-60(n1046)/+* animals (Figure G and H). *elt-3(0)* mutations did not contribute to *let-60*-dependent phenotypes consistent with a lack of significant ELT-3 expression in these cell types (Figure 3G).[15] Together, these results indicate

that *blmp-1* and *elt-3* function in a partially redundant manner to regulate diverse of developmental aspects, from animal morphology, to behavior to cell fate specification.

BLMP-1 and ELT-3 co-target overlapping gene sets

Our observations that *blmp-1* and *elt-3* genetically interact with *lin-42* to control the transcription of cyclically expressed miRNAs (e.g., *let-7*, Figure 1D) and that *blmp-1(0); elt-3(0)* double mutants exhibit pleiotropic defects led us to hypothesize that these TFs may function more broadly to control dynamic gene expression. To define the full repertoire of BLMP-1 and ELT-3 transcriptional targets, we complemented L1-staged BLMP-1 and ELT-3 ChIP-seq data obtained in the modENCODE project with additional ChIP-seq experiments performed in extracts made from L2-, L3-, and L4-staged animals.[24,25] Analysis of these combined data indicates that the regions bound by BLMP-1 in the first larval stage are also bound in subsequent larval stages. Furthermore, the binding sites of BLMP-1 in the L1-L4 stages significantly overlap with regions also bound by ELT-3 in the L1 stage (Figure 3A). A majority of BLMP-1 peaks are enriched within 500bps upstream of the transcriptional start site (TSS) but the enrichment also extends to 5' intergenic regions with a sharp drop-off approximately 3kb upstream of gene bodies of both protein coding and miRNA genes (Figure 3B and C). Peaks from all datasets were assigned to the nearest proximal gene (both coding and non-coding) using these parameters (Data S1A-E).

To characterize the relationship between BLMP-1, ELT-3 and their targets in more detail, we initially focused our analysis on protein coding genes whose expression can be reliably detected in developing larvae. Our analysis employed multiple, high-resolution, and genome-wide time course analyses of gene expression that parsed the larval developmental transcriptome into distinct temporal expression classes.[7,8] Both studies identified significant, overlapping sets of transcripts (between 12% and 18.9% of the transcriptome) that exhibit cyclical expression patterns. Hendriks et al. classified two types of dynamic expression: a first

class of transcripts that exhibit oscillatory or cyclical patterns (osc) that are tied to the molting cycle (osc; 18.9%; 2,718 of 14,378 total genes) or a second class of genes whose expression increases monotonically throughout larval development (rising; 14.2%) (Figure 3D). To compare how BLMP-1 and ELT-3 targets may be distinguished from the targets of other TFs, we analyzed additional publicly available ChIP-seq data sets obtained by the modENCODE project. This data included the targets of 170 additional *C. elegans* TFs that represent diverse classes of TFs.[24,25] Using the same target assignment criteria as above, we found that most TFs are associated with a limited number of target genes that exhibit a rising expression program (median targets bound = 21 per TF; interquartile range = 9 to 54)(Figure 3E; Data S2A). This relationship was also conserved for the associations between bulk TFs and the oscillatory class of target genes (median of 43 targets per TF; interquartile range = 18 to 97). Surprisingly, we found that a limited subset of 39 TFs is disproportionally associated with a large fraction of the oscillatory class of genes (Figure 3E). Primary amongst this unique group of 39 TFs were BLMP-1 and ELT-3 (with 1124 and 738 of the 2718 cyclically expressed targets bound per TF, respectively) (Figure 3E). Both BLMP-1 and ELT-3 binding sites are statistically enriched in the promoters of cyclically expressed genes (1124 osc BLMP-1 osc targets vs. 3265 non-osc targets and 738 ELT-3 osc targets vs. 2484 non-soc targets; $p < 0.0001$, Chi square test with Yates correction). We performed a similar analysis of the Kim et al. RNA-seq data to determine if ELT-3 or BLMP-1 binding sites are also enriched in the promoters of cyclically expressed transcripts as defined by their temporal classifications. Our analysis found that BLMP-1 binding sites, but not ELT-3 binding sites, are enriched in the promoters of each cyclically expressed genes class and de-enriched for those that exhibit monotonic expression patterns (Figure S3 and Data S2B).

One robust feature of cyclically expressed mRNAs is that the timing of expression within each larval stage occurs in the same phase of each transcriptional cycle. This expression/phase relationship is preserved even when animals are grown at lower or higher

temperatures which lengthens or shortens the periodicity of these patterns, respectively.[7,8] Because BLMP-1 and ELT-3 are constitutively expressed through each larval stage (Figure 3F), we aimed to determine if the subset of BLMP-1 and ELT-3 targets that exhibit cyclical expression patterns were concentrated in any particular phase of expression during each larval stage. To compare these patterns, we plotted the peak phase (in degrees/radians of a repetitive cycle) and expression level (log_2 change in expression as an increasing radius from the center) for each of the cyclically expressed transcripts on a radial chart (Figure 3G). ELT-3 and BLMP-1 targets were distributed across each sector of the repetitive temporal pattern and were not statistically enriched for any phase of expression. The distributed associations of these TFs and their varied targets combined with the constitutive expression of BLMP-1 and ELT-3 throughout each larval stage suggest that BLMP-1 and ELT-3 are associated with their targets throughout the transcriptional cycle regardless of transcriptional class of the target gene or their timing of expression.

Conserved sequences of the upstream regulatory regions of *lin-4* are necessary and sufficient for high amplitude expression in hypodermal tissues

Many of the heterochronic phenotypes associated with a null mutant of *lin-4, lin-4(e912),* can be partially rescued by a high-copy transformation of a 693bp genomic fragment that contains approximately 500bp of upstream putative regulatory sequence.[26] Analysis of the RNAs that are produced from the *lin-4* locus indicate transcription of *pri-lin-4* is initiated at least five TSS upstream of the *lin-4* gene.[27] Of these TSSs, three occur upstream of the minimal rescuing fragment, suggesting that additional regulatory information may be required to control normal aspects of *lin-4* transcription. These upstream regions are also associated with the active histone modifications H3K4me3 and open chromatin as measured by ATAC-seq assays (Figure 4A).[28,29] We compared the syntenic sequences of five additional nematode species to determine if regions of the F59G1.4 ninth intron were conserved through evolutionary selection.

This analysis revealed at least three discrete regions upstream of each *lin-4* gene that were disproportionately conserved when compared to similarly sized intronic and intragenic regions (Conserved Elements (CE) A, C and D). Examination of our ChIP-seq data indicate that each of these regions is enriched for BLMP-1 binding (Figure 4A, Data S1A-D). We did not detect a strong enrichment of ELT-3 bound to the putative *lin-4* regulatory sequences though multiple predicted ELT-3 consensus binding site sequences are found in this region (Figure 4A).

To test the functional relevance of these elements, we constructed a transcriptional GFP-pest reporter that harbors a SL2 splice acceptor sequence directly upstream of the GFP open reading frame (Figure 4A; Full Length (FL)). This feature enables each reporter to generate a single, defined mRNA transcript from each of the various candidate TSSs. This reporter is robustly expressed in a variety of cell types including the hypodermis, pharynx, body wall muscle, and ventral neurons on the surface of larva. Expression of the *lin-4::GFP-pest* reporter occurs once per larval stage (similar to other characterized transcriptional reporters) in these cell types indicating that this sequence contains the information to drive temporally and spatially restricted expression in multiple cell lineages. To characterize the temporal expression patterns in detail, we measured the levels of *lin-4::GFP-pest* expression in lateral seam cells at each of the morphologically defined stages of L4 development.[30] These experiments revealed that *GFP-pest* expression is highly pulsatile with expression peaking at the L4.5 and L4.6 stages (Figure 4B and C). Expression in other cell types (neuronal, pharynx, muscle and hyp7 cells) also peak during these larval substages with different expression trajectories (Data not shown). Specifically, muscle cells exhibit a broader (longer) transcriptional pulse compared to those observed in seam cells. Expression in hyp7 and neuronal cell types exhibit a shorter pulse of transcription either muscle or seam cells (Figure 4B).

We then compared the expression patterns we observed using the full-length construct to previously published reporters or variants of the full-length reporter that lack individual or combinations of the conserved sequence elements outlined above. Each of the reporters

express pulses of GFP-pest expression in similar cell types as the full-length version.[5,27] However, peak expression in the hypodermal cells was typically 5-20-fold higher from the full-length reporter compared to the other derivative reporter genes (Figure 4D). Deletion analyses of the full-length construct indicate that CE A, harboring sequences that bind BLMP-1 *in vivo*, are primarily responsible for this increased transcriptional output as reporters that lack this element exhibit residual expression to a similar level as the minimal rescuing fragment (Figure 4D and E).

Using the ChIP-seq data sets for BLMP-1::GFP, we identified a consensus sequence for BLMP-1 that is enriched in the CE A regulatory sequence (Figure 4A and C). A recombinant GST translational fusion of the five BLMP-1 zinc fingers (ZnFs), GST-BLMP-1(ZnFs), but not GST alone bound several sequences found in CE A element that conform to this consensus. This binding was diminished by the addition of cold competitor DNA harboring consensus BLMP-1 binding sites but not by a similar sized, non-specific target DNA (Figure 4G). To determine if these elements function as a transcriptional enhancer, we cloned a 138bp fragment from the CE A element, called minimal CE (minCE) (Figure 4A and H), into the 5' regulatory sequences of the *gst-5* gene encoding the *C. elegans* ortholog of human HPGDS (hematopoietic prostaglandin D synthetase). RNA-seq experiments demonstrate that *gst-5* mRNAs are expressed throughout larval development in a variety of tissues (including the hypodermis) and exhibit a non-cyclical or flat expression pattern.[7,8,15] A transcriptional reporter bearing 2.9kb of the *gst-5* upstream regulatory sequences drives a low level GFP-pest expression in a number of larval cell types including the pharynx, intestine, neurons and hypodermis and this expression pattern remained below the threshold of imaging during normal development (Figure 4H). In contrast, the transcriptional reporter that included two copies of the minCE in the reverse orientation (reversed compared to the orientation within the *lin-4* enhancer element) drove high amplitude, periodic expression of GFP-pest exclusively in hypodermal cells (Figure 4H). Expression of the *(2xminCE)gst-5::GFP-pest* reporter in *blmp-*

1(0) mutant animals resembled the expression of the simple, *gst-5::GFP-pest* reporter in wild-type animals (Figure S4), consistent with the hypothesis that this minimal sequence from the *lin-4* upstream region functions as both a spatial and temporal enhancer.

BLMP-1 controls the transcriptional output of its targets

A large fraction of BLMP-1 and ELT-3 targets are expressed in a cyclical fashion (approximately 26% and 23%, respectively) (Figure 3D and Data S2A). We reasoned that targets that exhibit this highly dynamic form of gene expression could provide an opportunity to determine the effects of BLMP-1 and/or ELT-3 binding on transcriptional dynamics in more detail. To quantify changes in expression dynamics, we obtained or constructed integrated transcriptional GFP-pest reporters that fit three criteria. First, we identified candidate genes that are predicted to be targets of BLMP-1 and/or ELT-3 as measured by ChIP-seq (Figure 3 and Figure S2). Second, we selected genes that are predicted (by RNA-seq experiments) to be dynamically expressed in hypodermal tissues.[15] Third, we selected a set of genes whose expression peaks are predicted (again, by RNA-seq experiments) to occur at a variety of phases within the molting cycle.[8] Based on these criteria, we constructed or obtained multi-copy integrated transcriptional GFP-pest reporters for *(2xminCE)gst-5, moe-3, mlt-10,* and *ZK180.5* and a single copy version of a transcriptional GFP-pest reporter for *C02E7.6* integrated on chromosome II. To characterize the temporal expression patterns of these reporters, we assembled a series of measurements that spanned the morphologically defined stages of L4 development. As shown in Figures 5A-C, each reporter is expressed in a pulsatile expression pattern with *(2xminCE)gst-5* and *C02E7.6* reporters exhibiting a peak of expression in the mid-L4 stage, and the *moe-3* transcriptional reporter reaching maximal amplitude near the end. We next aimed to determine how mutations in *blmp-1* and/or *elt-3* altered these expression patterns. GFP-pest expression levels in seam cells were then quantified in each genetic context at a developmental stage where reporter expression peaks in wild-type

346 animals. As illustrated in Figure 5A and B, *blmp-1(0)* mutations dampen the expression of both
347 *(2xminCE)gst-5* and *C02E7.6* reporters by approximately 1.7-fold. In contrast, *elt-3(0)*
348 mutations had little effect on the transcriptional output of either of these two reporters.
349 Furthermore, the decrease in seam cell expression for the *(2xminCE)gst-5* and C02E7.6
350 reporters was not further decreased in *blmp-1(0); elt-3(0)* double mutants, consistent with a
351 lack of ELT-3 binding sites in these promoters. In contrast, examination of *moe-3::GFP-pest*
352 expression in various mutant backgrounds indicate that activity of both *blmp-1* and *elt-3* are
353 required to maintain high transcriptional output for this gene in the hypodermis (Figure 5C).
354 We next sought to correlate dynamic changes in gene expression to other aspects of
355 larval development in more detail. To accomplish this, we performed long-term, live imaging of
356 developing larvae in a microfluidic device[31], enabling us to continuously monitor gene
357 expression dynamics in individual animals and also correlate this dynamics with other cellular
358 and developmental milestones. We focused on two of the most strongly expressed reporter
359 genes, *mlt-10pro::GFP-pest* and *zk180.5pro::GFP-pest*, both exclusively expressed in the
360 hypodermis (Figure 5D) and their respective putative regulatory elements bound by BLMP-1
361 and ELT-3 (Figure 3 and Figure S6). First, we compared overall developmental pace between
362 WT, *blmp-1(0)*, *elt-3(0)* and *blmp-1(0);elt-3(0)* animals in the microfluidic chambers by
363 assessing the time between the successive ecdysis (cuticle shedding). While both WT and
364 mutant animals displayed variability of larval stage duration within each genotype, neither
365 *blmp-1(0)* nor *elt-3(0)* mutations (or combination of these mutations) affected the average
366 duration to a substantial degree (Figure 5E and Figure S5). However, our live imaging
367 experiments revealed a partially penetrant larval lethality phenotype, in particular in the L3
368 stage, that was not apparent on standard, solid NGM plates.
369 The fact that the larval stage durations are largely preserved between WT and *blmp-*
370 *1(0)/elt-3(0)* mutants allowed us to directly compare average quantitative temporal features of
371 transgene gene expression dynamics such as the time within each transcriptional cycle in

372 which transcription begins, peak phase (the point within each cycle in which the peak
373 expression is reached), and the cumulative accumulation of GFP-pest expression (output)
374 between genetic backgrounds. To this end, we extracted individual whole-animal fluorescence
375 time course measurements and rescaled them such as to align the timing of molting events of
376 each animal (see Methods) to the average WT molting times (Figure 5F). Consistent with other
377 *blmp-1-* or *blmp-1; elt-3*-dependent reporters, cyclical transcription of *ZK180.5::GFP-pest* and
378 *mlt-10::GFP-pest* was maintained throughout larval development indicating that *blmp-1* (or *elt-*
379 *3)* are not essential for generating pulsatile patterns of transcription (Figure 5F-J and Figure
380 S6). The primary difference between the expression trajectories of wild type and mutant
381 animals was the drastic reduction in the amplitude of individual traces in *blmp-1(0)* mutants.
382 Surprisingly, the reduction of transcriptional output was not accompanied by any substantial
383 change in the timing of transcriptional induction (Figure 5H and J and Figure S6). Ultimately,
384 the reduction of transcriptional output (as measured by total cumulative GFP-pest expression
385 during each pulse) correlates with a reduction in the relative duration of expression in mutant
386 animals (Figure 5H and J and Figure S6). These results indicate that BLMP-1 functions to
387 amplify the baseline pulsatile transcriptional dynamics that are likely generated by other gene
388 regulatory mechanisms. With respect to the *(2xminCE)gst-5::GFP-pest* reporter (see above),
389 our findings suggest that the 138bp minCE fragment may contain the regulatory sequences
390 required by these mechanisms to generate oscillatory transcription but the resulting oscillation
391 amplitude is strongly dependent on BLMP-1 binding.
392
393 **The *lin-4* locus adopts a BLMP-1-dependent, active chromatin structure in hypodermal**
394 **cells**
395 Previous studies indicate that BLMP-1 physically and functionally interacts with multiple
396 chromatin remodeling factors (e.g., SWI/SNF subunits) and that BLMP-1 binding sites are
397 enriched in open chromatin regions (Figure S2).[28,29,32] We hypothesized that BLMP-1 may

function to potentiate transcription through chromatin remodeling near its binding sites which would potentiate the binding of additional TFs. This model would account for the dependency of the diverse transcriptional targets of BLMP-1 that differ in their temporal pattern of expression (phase) during the repetitive transcriptional cycle and would be mechanistically similar to the activities of other TFs (including pioneer factors) that remodel chromatin accessibility prior to the onset of major transcriptional induction in *C. elegans*.[33-35]

We therefore sought to measure how BLMP-1 activity may alter chromatin dynamics at a specific locus with spatiotemporal resolution. We utilized an established chromosome-tagging strategy that has been employed to visualize both the localization of transgenic arrays and dynamics of chromatin compaction in living animals.[33,36,37] Transgenes containing the *lin-4(FL)::mCherry-pest* ORF flanked by tandem copies of the bacterial lac operator (lacO) sequences were integrated to a single chromosomal site and then crossed into a strain harboring a soluble, ubiquitously expressed GFP-tagged lac repressor (LacI) fusion that recognizes lacO sequences with high affinity.[35] The enabled us to monitor the *lin-4* locus in live animals while simultaneously monitoring transcriptional output of the *lin-4* enhancer/promoter (Figure 6A). Animals harboring these transgenes exhibit two foci in each somatic nucleus indicating the stable, single integration site of the *lin-4::mCherry/LacO* transgene. The intranuclear GFP-LacI foci found in freshly hatched L1-staged animals can be grossly categorized into two basic classes: Class 1) a punctate or “ball-like” pair of GFP-LacI foci that are found in a majority of somatic cells and Class 2) pairs of “puffed” foci that are found in the nuclei of hypodermal cells (Figure 6B). This lineage-specific decompaction of the *lin-4* locus is surprising for multiple reasons. First, *lin-4* loci appear to be decompacted only in hypodermal tissues where BLMP-1 is normally expressed. Second, chromatin decompaction is typically associated with active transcription in a variety of systems[38-40] and the decompaction of the *lin-4* loci in freshly hatched L1-stage animals precedes any detectible *lin-4::mCherry-pest* expression (Figure 6B).

To test whether BLMP-1 expression correlates with target loci decompaction, we performed two types of analyses. First, we characterized when BLMP-1 expression begins in embryos. BLMP-1::GFP can be detected as early as the bean stage (approximately 365 minutes post fertilization) in most developing hypodermal cells (Figure 6C). This tissue-specific expression pattern remains throughout the rest of embryonic development (Figure 6C). We next aimed to determine how the timing of BLMP-1 expression correlates with the decompaction level of the *lin-4* loci by examining changes in GFP-LacI foci. From the onset of GFP-LacI expression to the early gastrulation stage of embryogenesis, most somatic *lin-4* GFP-LacI foci are decompacted, consistent with a general lack of condensed chromatin and reduced histone H3 lysine 9 (H3K9) methyltransferase activity in early embryos.[40-43] By the end of gastrulation (approximately 330 minutes post fertilization) the foci in most somatic cells are equally condensed consistent with the onset of large-scale heterochromatin formation in somatic cells and a reduction in transcriptional plasticity.[40-42] At roughly the same time as the onset of BLMP-1 expression in embryonic hypodermal cells, the GFP-LacI foci begin to decompact in posterior seam cells (Figure 6D). The cell type-specific decompaction of *lin-4* loci in hypodermal tissues is complete for a majority of wild-type animals by the end of embryogenesis while the same foci in other somatic cell types remain tightly compressed (Figure 6D). GFP-LacI foci dynamics were similar in wild-type and *blmp-1(0)* animals during early embryogenesis. In contrast to the late embryonic decompaction of *lin-4* loci in wild-type animals, hypodermal GFP-LacI foci (and foci in other somatic nuclei) in *blmp-1(0)* mutants remained condensed (Figure 6D and E). We conclude that BLMP-1 is required for decompaction of the *lin-4* loci in hypodermal cells during embryogenesis. Furthermore, this decompaction occurs at a point in development where *lin-4* transcription is being actively repressed by multiple FLYWCH proteins[44] and transcriptional activity is undetectable with our fluorescent transcriptional reporter; though minimal transcription during this period cannot be excluded.

We next aimed to directly monitor any dynamic changes in “puffs” sizes within the transcriptional cycle of *lin-4* during larval development and determine if these changes are dependent on BLMP-1 activity. In head ganglion cells, derived from a cell lineage that never express the *lin-4pro::mCherry-pest* transgene, the two *lin-4pro::mCherry-pest* loci are constitutively compacted (Figure 6F and G). To measure changes in cells that do express *lin-4* miRNAs, we focused our analysis on developing lateral seam cells for multiple reasons. First, seam cells constitutively express BLMP-1 and dynamically express the *lin-4pro::mCherry-pest* reporter at specific phases of each larval stage (Figure 1B and Figure 4A). Second, in contrast to hyp7 syncytial cells that endoreduplicate their nuclear DNA content at each division resulting in a stable ploidy of 4n, seam cells replicate their nuclear DNA once per division at specific, defined phases of the larval molt cycle.[45] To ensure accuracy in both the timing of *lin-4::mCherry-pest* expression and seam cell divisions, we specifically measured the compaction status of the *lin-4::mCherry-pest* loci in late L3-staged animals where morphological features of the vulval cell lineage, gonad morphology, and *mCherry-pest* expression could be used to compare animals of both genotypes at similar developmental stages. We found that the GFP-LacI “puffs” size lateral seam cells with undetectable *lin-4pro::mCherry-pest* expression was typically three times larger than those found in neurons (Figure 6F and G). Later, during the L3 lethargus, when *lin-4pro::mCherry-pest* is expressed, we observed that the average size of the GFP-LacI “puffs” further increase in size (approximately an additional 2-fold when compared to seam cells lacking *lin-4pro::mCherry-pest* expression) (Figure 6F and G). This suggests that the *lin-4* locus is constitutively decompacted (compared to the same locus in neuronal cells) and the process of transcribing this locus further relaxes chromatin architecture. We then asked if chromatin decompaction at these loci was dependent on BLMP-1 activity by examining the same features in *blmp-1(0)* animals. A comparison of the GFP-LacI “puff” sizes in head neurons indicates that they are equally compressed in wild-type and *blmp-1(0)* animals (Figure 6F and G). In contrast, GFP-LacI foci, in both non-transcribing and *lin-4* expressing cells, are

significantly reduced in size compared to those observed in stage-matched wild-type animals (Figure 6F and G). These experiments demonstrate that the chromatin structure of the *lin-4* locus is dynamically remodeled in seam cells and that BLMP-1 is required for decompaction of the *lin-4* locus in hypodermal cells prior to high-amplitude transcription in wild-type, larval animals.

BLMP-1 and ELT-3 are required to resume normal temporal patterning after nutrient deprivation

Development of *C. elegans* larvae in laboratory conditions is both rapid and continuous due to an abundant, controlled food supply and standardized growth conditions. In contrast, the natural environment in which *C. elegans* larvae normally live is far more diverse and dynamic leading to a more punctuated developmental trajectory.[46] Acute food removal induces a defined developmental diapause that can occur immediately after each larval molt.[47] The diapause is part of a developmental checkpoint that is distinct from dauer development and controlled by insulin signaling.[47] When insulin signaling becomes rapidly inactivated (i.e. during acute starvation), animals finish the current larval stage, including somatic cell divisions and the molt, but then arrest all somatic cell movements and divisions, and suspend the subsequent expression of molting-specific genes.[47]

To determine if global aspects of cyclical transcription are altered during acute starvation, we monitored the expression of four transcriptional reporters that exhibit distinct phases of expression (Figure 5). These reporters include targets of BLMP-1 and ELT-3 (*(minCE)gst-5::GFP-pest*, *ZK180.5::GFP-pest,* and *mlt-10::GFP-pest*) as well as a transcriptional reporter of *blmp-1,* since ChIP-seq data indicates that it is expressed in a cyclical expression pattern[7,8] and BLMP-1 activity regulates its own expression through direct positive feedback (Figure S7). We grew populations of L1-staged animals under nutrient-rich conditions for 22 hours and then one half of each sample was allowed to continue development

in nutrient replete conditions while the other half was acutely starved (Figure 7A). Acute food removal results in greater than 90% of transgenic animals arresting development with undivided vulval precursor cells after 24 hours indicating that larval development has been paused.[47] During the starvation period, we monitored GFP-pest expression in fed and starved populations. In contrast to the cyclical expression of each reporter under nutrient replete conditions, GFP-pest expression for each of the reporters was extinguished during starvation conditions with similar kinetics (Figure 7B). This transcriptionally inactive state was maintained throughout the starvation period. Re-fed animals resumed normal, cyclical expression patterns within a few hours after food exposure (Figure 7B). These experiments demonstrate that oscillatory transcription is inhibited by the starvation-induced developmental diapause and that wild-type animals can re-initiate these transcriptional patterns in a nutrient-dependent manner.

BLMP-1 expression is actively regulated post-translationally by a conserved F-box protein, DRE-1, that mediates the ubiquitination of target proteins which are degraded by the proteasome.[16] Given that *blmp-1* is cyclically transcribed and its transcription is inhibited in nutrient depleted conditions (Figure 7B), we hypothesized that the constitutive expression of BLMP-1 during normal development may be altered during starvation. To test this, we repeated the nutrition-mediated arrest experiments outlined above in strains harboring BLMP-1::GFP and ELT-3::GFP translational fusions. The expression patterns of each translational fusion were compared to a constitutively expressed monomeric GFP transgene (*sur-5::GFP*) to control for potential changes in GFP half-life under starvation conditions. Surprisingly, BLMP-1::GFP expression was diminished during starvation with >50% of animals loosing detectible BLMP-1::GFP expression after 12 hours of starvation. In contrast to the down-regulation of BLMP-1::GFP, most starved animals retained ELT-3::GFP and soluble GFP expression throughout the starvation period with only a mild reduction after 24 hours (Figure 7C). As with the transcriptional reporter for *blmp-1* expression, BLMP-1::GFP expression was detectible again in most animals within 2 hours or re-feeding and resumed normal, pre-starved

528 expression levels after 5 hours (Figure 7C). Similar changes in *blmp-1* mRNA and BLMP-1
529 protein expression were seen in freshly hatched and starved L1 (Figure S8). We conclude that
530 BLMP-1 expression, both transcriptionally and post translationally, is regulated by nutrient
531 availability.

532 To examine if BLMP-1-dependent chromatin remodeling is also modulated by nutrient-
533 dependent signaling, we monitored compaction of *lin-4* locus in animals that have entered the
534 acute starvation-dependent developmental diapause. At the mid-L3 stage (first VPC division), a
535 developmental time point that precedes *lin-4* transcription during the L3 stage the *lin-4* locus
536 was decompacted (Figure 7D). We then rapidly removed the bacteria food source to induce the
537 L4-specific developmental diapause. After 22 hours of starvation, >90% of animals arrested at
538 the invagination stage of vulval development (L4.1-L4.2) which precedes fusion between the
539 anchor cell and vulval precursor cells on the ventral surface of the L4 larva.[30] Analysis of lateral
540 seam cell GFP-LacI puffs sizes in starved animals demonstrated that the *lin-4* loci in seam cells
541 were dramatically compacted when compared to the same loci in continuously developing
542 animals (Figure 7D). Re-plating of these starved animals lead to the rapid decompaction of the
543 *lin-4* locus at a timepoint with BLMP-1 expression has resumed (Figure 7D). Interestingly, the
544 level of decompaction is greater in recovering animals that those found in non-starved,
545 continuously developing animals (Figure 7D). We also monitored *lin-4::mCherry*/LacO loci in
546 the seam cells of starved, L1-stage animals and also found that loci compacted in these
547 starvation conditions (Figure S7). In sum, these experiments indicate that dynamic chromatin
548 rearrangements are modulated by nutrient sensing.

549 Changes in BLMP-1 expression and the dramatic compaction and decompaction of
550 BLMP-1 target chromatin during starvation and recovery, respectively, suggests that BLMP-1
551 could play an essential role in modulating transcriptional output of critical developmental genes
552 in dynamic environments. To determine whether animals that lack *blmp-1* and/or *elt-3* can
553 robustly adapt to starvation, we repeated the food experiments as described in Figure 7A but

maintained the animals in starvation conditions for increasing periods of time. At the end of the starvation period, animals were re-plated on normal food and monitored for developmental phenotypes by scoring changes in *col-19::GFP* expression when the animals had reached adulthood (Figure 7E). In these experiments, wild-type and *elt-3(0)* larvae re-initiate normal temporal patterning after prolonged bouts of starvation (Figure 7E). In contrast, a minor fraction of *blmp-1(0)* mutants failed to express *col-19::GFP* in hyp7 cells, a phenotype associated with weak reiterative heterochronic mutants.[17,48] The relatively mild *blmp-1(0)* phenotypes were dramatically enhanced in *blmp-1(0); elt-3(0)* double mutants. These results indicate that BLMP-1 and ELT-3 are essential for resuming normal temporal patterning after continuous development has been interrupted by starvation.

Discussion

Features of the oscillatory expression program impose constraints on modulating transcriptional output

Oscillatory patterns of gene expression are a ubiquitous feature of developmental systems where they orchestrate repetitive biological functions and/or anticipate recurring environmental conditions.[49] While most GRNs that program cyclical patterns of gene expression utilize a basic negative feedback structure, specific features of their architecture define the precision of the timekeeping mechanism and the ability to modulate and/or preserve features of dynamic transcription. For instance, the periodicity of circadian gene expression persists in the absence of external cues over a wide range of temperatures, yet changes in lighting or nutrition can alter the phase of gene expression or the amplitude of clock target gene transcription, respectively.[50,51] The genetic control of plant root formation also employs a complex feedback loop that generates cyclical transcriptional cycles that induce the formation of lateral roots at periodic positions along the radial surfaces of the developing primary root. The transcriptional output of this GRN is modulated by a hormone, auxin, that amplifies oscillatory transcription in

a dose-dependent manner.[52] Exposure to light is required for maintaining the oscillatory transcriptional patterns at the pre-branch sites.[53] Water availability can also modulate the ability to the root clock to induce lateral root founder cell development. Uneven water distribution on the surface of the developing primary root leads to a suppression of LR development on the dryer root surface. Importantly, changes in water distribution do not alter the cycling of core root clock components indicating the environment can control clock output at the phenotypic level.[54]

While the molecular components of the *C. elegans* expression oscillator are not fully known, a detailed characterization of the systems-level behavior of this GRN indicates that two features are hard-wired. First, the biological oscillator is directly tied to the molting cycle and gated by genetically-regulated developmental checkpoints.[8,47,55] Under replete nutritional conditions, transcriptional cycling is continuous.[8] Removal of food either at hatching or just prior to the termination of the molt results in a regulated arrest of the developmental clock at a precise point within the transcriptional cycle (Figure 7B).[8] Re-initiation of the transcriptional clock (either from starved L1-stage animals, dauer arrest, or the nutrition-mediated arrest points at each larval stage) occurs at this same point.[8] These features indicate that once initiated, the transcriptional cycle is modular in nature and progresses until the next checkpoint. Secondly, the periodicity of thousands of cyclically expressed transcripts scales inversely with temperature over a wide dynamic range and the relative timing of expression for individual genes within the transcriptional cycle is phase-locked.[7,8]

Because the accordion-like, modular structure of this GRN constrains the relative timing of transcriptional events within the cycle, other features of cyclically transcribed genes are likely modulated independently of the clock. This adaption of transcriptional output to various environments would be especially important for genes that are expressed at determinant phases within the transcriptional cycle and function in dosage-sensitive manners. This feature is exemplified by the heterochronic miRNAs that exhibit pulsatile transcriptional patterns at

each larval stage and also function to control discrete transitions of temporal cell fate at specific developmental milestones (molting).[56] It had been previously shown that LIN-42, the *C. elegans* Period ortholog, functions to limit transcriptional output of this class of genes by negatively regulating the overall duration of transcription within each larval stage.[5,6,12] In this manuscript, we present evidence that BLMP-1 functions to antagonize LIN-42 activities by increasing the duration of transcription for cyclically expressed genes. As with *lin-42, blmp-1* is not essential for the generation of cyclical expression patterns but plays a modulatory role in controlling the duration and amplitude of transcription (Figure 7G). How the interplay between these two antagonistic modulators of gene expression achieves precise tuning of gene-dosage to confer robustness and adaptivity to post-embryonic developmental programs is an exciting route for further investigation given that BLMP-1 targets the *lin-42* locus (Data S1A-D).

BLMP-1 couples chromatin de-compaction and the regulation of transcriptional output

In *C. elegans*, BLMP-1 is known to physically interact with chromatin remodeling components (SWSN-1, a core component SWI/SNF of the complex (orthologous to human SMARCC1/BAF155) and HAM-3, an accessory subunit of the SWI/SNF complex) suggesting that BLMP-1 may direct these activities in a sequence-specific manner.[32] Mouse Blimp-1 has been shown to alter transcriptional activity of target genes by recruiting chromatin remodeling and histone modifying complexes.[57] The physical associations are conserved between the human ortholog of BLMP-1, hBlimp1, and the hSWI/SNF complex; suggesting additional features of BLMP-1 function may be shared. Here, we characterize a molecular role for BLMP-1 in regulating the transcriptional output of a number of cyclically expressed genes in *C. elegans* through a mechanism involving the decompaction of chromatin near its target gene loci. In contrast to the chromatin decompaction that occurs during normal transcriptional activation[38-40], we demonstrate that

BLMP-1-dependent decompaction is temporally separated from the activation of the target gene expression and can occur even when transcription is actively repressed by other mechanisms (e.g. for the *lin-4* gene during embryogenesis (Figure 6B and D).[44] We hypothesize that this anticipatory priming mechanism constitutively opens chromatin loci near BLMP-1 binding sites. These "primed" loci would then be accessible to additional TFs whose binding capacity may be normally restricted by nucleosome complexes. Once bound, these factors would induce the phased patterns of gene expression that define the transcriptional cycle for each target gene (Figure 7 G). Because BLMP-1 binding sites are associated with a multitude of genes that are expressed in diverse phases of the oscillatory transcriptional pattern (Figure 3), we speculate that the BLMP-1-dependent "priming" activity is not limited to a single partner TF but likely facilitates the association of several TFs that function at distinct phases of the transcriptional cycle. In the absence of BLMP-1, many of these factors would exhibit a reduced capacity to bind to their cognate binding sites. As a result, *blmp-1(0)* mutants exhibit broad changes in transcriptional dynamics. The diversity of these changes would result in pleiotropic phenotypes whose only common feature would be a change in gene dosage across multiple GRNs. Notably, while our analysis focused on genes whose overall expression is upregulated in the presence of BLMP-1, the mechanism we propose by which BLMP-1 modulates target transcription is equally capable of inhibiting transcription of target genes (by increasing chromatin accessibility for transcriptional repressors).

The molecular mechanism that we propose for BLMP-1 in temporal gene regulation is analogous to the role that the TF Zelda (ZLD) plays in establishing normal spatial gene regulation during *D. melanogaster* embryogenesis. In this system, ZLD is ubiquitously expressed throughout the embryo where it functions as a pioneer factor to rearrange chromatin near its binding sites.[58-60] Spatially ubiquitous ZLD activity facilitates the transcriptional activation of genes that are co-targeted by the transcription factor Dorsal (DL). Unlike ZLD, DL is expressed in a dorsal-ventral gradient that extends from the dorsal surface of the embryo to

656 the lateral edge. DL functions in a dosage-dependent manner to generate a graded expression
657 of target genes.[61,62] Mutation of ZLD binding sites in DL-dependent reporter transgenes results
658 in the dramatic compression of reporter gene expression along the dorsal-ventral axis.[63]
659 Importantly, *zld* mutations do not alter DL distribution along the dorsal-ventral axis suggesting
660 that ZLD activity primes DL targets by reorganizing chromatin architecture that would otherwise
661 impair DL binding and function. As with mutations of BLMP-1 in the context of temporal gene
662 expression, *zld* mutations additionally alter the duration of DL target expression.[63]
663
664 **Regulation of BLMP-1 expression in response to nutrient availability coordinates**
665 **transcriptional output**
666 We hypothesize that the re-initiation of transcription after starvation elicited by food is essential
667 for animals to re-format the chromatin landscape near their target genes after quiescence and
668 to rapidly modulate the transcriptional output of genes that control temporal patterning. In this
669 manuscript we also show that *blmp-1* expression is regulated by nutrient availability and is
670 important for the coordination of transcriptional output in a variety of conditions. Under
671 nutritionally replete growth conditions, *blmp-1* transcription is both cyclical and auto-regulatory.
672 While *blmp-1* expression at the mRNA level is highly dynamic, BLMP-1 protein expression is
673 highly stable and maintained at relatively constant levels during continuous growth.[7,8,16]
674 Starvation elicits two main changes in *blmp-1* expression that directly lead to a reduction in the
675 priming activity. First, the cyclical transcription of *blmp-1* (as with most other cyclically
676 expressed genes) is arrested when animals pause development at a starvation-induced
677 developmental checkpoint. Second, BLMP-1 expression is rapidly curtailed during starvation.
678 BLMP-1 expression is likely dampened by the combined reduction in transcription and the
679 constitutive activity of DRE-1 that functions independently of starvation.[16] This reduction of
680 BLMP-1 expression is coincident with a re-compaction of chromatin near BLMP-1 target genes.
681 The establishment of non-permissive chromatin architecture may be a common feature of

682 quiescent cells as diverse cell types (from yeast to human cells) exhibit these changes. It has
683 also been previously suggested to control inappropriate transcription in the context of
684 development.[64-69] The regulation of BLMP-1 expression through nutrient availability is also
685 important for the coordination of gene expression after starvation as *blmp-1(0)* and *blmp-1(0);*
686 *elt-3(0)* animals fail to resume normal temporal patterning after starvation.
687 Finally, we hypothesize that the active control of BLMP-1 levels/activities may be
688 important for the adaption of global transcriptional patterns to the environment. The separate
689 genetic control of transcriptional timing and transcriptional output would enable gene
690 expression dynamics to be optimized to specific conditions and ensure developmental
691 robustness. Evidence that the levels of BLMP-1 protein are actively regulated are derived from
692 the observation that *dre-1(lf)* phenotypes result in an inappropriate over-expression of BLMP-1
693 and a coincident increase in precocious developmental phenotypes.[16] The active control of
694 BLMP-1 protein expression may play an important role in the adaptation of transcriptional
695 output to different temperatures where the periodicity of the transcriptional cycles and
696 developmental pace changes dramatically.[7,8] This homeostatic strategy, mediated by
697 controlling the expression of a single pioneer transcription factor, could buffer differences in
698 transcriptional dynamics across the transcriptional cycle by modulating chromatin accessibility.
699

ACKNOWLEDGEMENTS

We thank A. Zinovyeva, V. Ambros, L. M. Kutscher, and members of the Hammell laboratory for critical review of this manuscript. We received *C. elegans* strains and recombinant DNAs from S. Gasser, O. Hobert, L. Cochella. The ATIP/Avenir Young Investigator program of the CNRS supported to W.K. W.K. initiated and performed part of this work while being a postdoctoral fellow in the laboratories of Shai Shaham (S.S.) and Eric D. Siggia (E.D.S) at Rockefeller University, supported by NIH grant R35NS105094 to S.S., NSF grant PHY 1502151 to E.D.S. and a postdoctoral fellowship (LT000250/2013-C) from the Human Frontier Science Program (HFSP) to W.K.. Cold Spring Harbor Laboratory, the Rita Allen Foundation, HIH NIGMS R01GM117406 supported C.M.H..

AUTHOR CONTRIBUTIONS

N.S., W.K., and C.M.H. designed, performed and analyzed most experiments and wrote the manuscript. ChIP-seq experiments were performed by V.E. and S.E.. C.M.H and K.H-M. analyzed sequencing data. Gel shift experiments were carried out by K.D.. Reporter construction and gene expression analysis was carried out by C.M.H., N.S. and K.D.. Microfluidics experiments were carried out by W.K.. Starvation experiments and LacO/LacI experiments were carried out by N.S. and C.M.H..

DECLARATION OF INTERESTS

The authors declare no competing interests

Figure 1. *blmp-1* and *elt-3* antagonize *lin-42* activity to control the expression of heterochronic miRNAs.

(A) Representative *col-19::GFP* expression patterns in wild-type, *lin-42(lf), blmp-1(0); lin-42(lf),* and *blmp-1(0); lin-42(lf); elt-3(0)* animals.

(B) A quantification of the *col-19::GFP* expression phenotypes of various mutant combinations in L4- and adult-staged animals.

(C) Expression patterns of BLMP-1::GFP and ELT-3::GFP transgenes in hypodermal cells. Sn = Seam cell nuclei.

(D) SCM::GFP is expressed in lateral seam cells and can be used to monitor cell division patterns during larval development. Mid-L4-staged *alg-1(0); blmp-1(RNAi)* animals exhibit a supernumerary number of SCM::GFP cells.

(E) Quantification of lateral seam cell numbers of mid-L4-staged animals exposed to bacteria expressing dsRNAs complementary to *elt-3, blmp-1* or both *blmp-1* and *elt-3*. Red bars indicate mean and SEM. Asterisks indicate statistically significant differences in phenotype ($p = < 0.0001$) calculated from a two-tailed chi-square analysis. $n = > 40$ animals per genotype/RNAi condition.

(F) Lateral seam cell lineage of wild-type, *blmp-1,* and *alg-1* mutants and experiments outlined in panel F. See also Figure S1.

Figure 2. *blmp-1* and *elt-3* regulate several additional morphological, behavioral, and cellular phenotypes.

(A) *blmp-1(0); elt-3(0)* animals exhibit a synthetic Dpy phenotype that manifests during larval development.

(B) Quantification of animal length-to-width ratio in freshly hatched larvae (left) and young adult animals (right) of the indicated genotypes ($n = >20$). Red bars indicate the mean and SEM.

(C) *blmp-1(0)* and *blmp-1(0); elt-3(0)* animals prematurely die after the L4-adult transition.

(D) The lethality of *blmp-1(0); elt-3(0)* adult animals correlates with an inability to shed the cuticle of a supernumerary molt.

(E) *blmp-1(0); elt-3(0)* inappropriately reanimate the expression of a *mlt-10::GFP-pest* transcriptional reporter during adulthood. Animals were imaged at the L4-adult transition or as gravid adults.

(F) Major components of the vulval induction pathway (see text for details). Components that are genetically involved in vulval induction are colored green whereas those involved in

Notch/lateral inhibition are colored black. The *let-7* family miRNA miR-84 (red) that regulates *let-60* expression is temporally expressed in presumptive secondary fate vulval cells.

(G) *blmp-1(0)* mutations enhance the expressivity and penetrance of *let-60(n1046gf) muv* phenotypes. Animals of the indicated genotypes were scored for the number of vulval protrusions present on the ventral side at the young adult stage (n = >90). Brackets indicate statistically significant differences in phenotype calculated from a two-tailed chi-square analysis.

(H) Representative images depicting *muv* phenotypes associated with the indicated genotypes.

Figure 3. BLMP-1 and ELT-3 bind similar sites in the genome and are associated with the putative regulatory regions of gens that exhibit cyclical expression patterns.

(A) A matrix of global pairwise factor co-association strengths as defined by promoter interval statistics indicate that BLMP-1 and ELT-3 bind similar genomic regions.

(B) The distribution of the peak summit positions of BLMP-1 ChIP-seq data mapped relative to the TSS of protein coding genes or to the +1 nucleotide of the DNA sequence encoding the miRNA precursor RNA.

(C) A heat map of ChIP-seq signals +/- 3 kb centered on the TSS of each of the 14,252 protein coding genes measured in the developmental RNA-seq data set.[8] Genes are organized for each heat map in a 1:1 fashion according to their density of unique reads present in the BLMP-1 L1-stage ChIP-seq sample (see Data S1).

(D) The *C. elegans* larval transcriptome can be categorized into two dynamic expression classes (rising and oscillating) that are distinct from the predominantly flat expression pattern of most mRNAs (grey region; 66.9%).[8]

(E) A graph displaying the number of predicted rising or oscillating class targets for each of the 172 TFs assayed by the ModEncode Projects (data derived from a total of 265 ChIP-seq data sets assayed). Red bars indicate the median (thick) with the interquartile range (thin). Numbers in parenthesis indicate ranks of BLMP-1 or ELT-3 among all TFs (Data S2 and Figure S3).

(F) Quantification of GFP intensity for translational reporters of BLMP-1 and ELT-3 during the L4 stage.

(G) A radar chart plotting oscillation amplitude over the phase of peak expression reveals that BLMP-1 and ELT-3 bind the putative regulatory regions of periodically expressed genes in all phases of the cyclical transcriptional cycle (see Data S1).

See also Figure S2.

Figure 4. Conserved elements in the *lin-4* promoter are both necessary and sufficient for high-amplitude expression in hypodermal tissues.

(A) A browser track overlaying the predicted BLMP-1 consensus binding sites, the BLMP-1::GFP ChIP-seq signal from L1-staged larvae, and conservation of these sequence features found in *C. elegans, C. brenneri, C. tropicalis, C. remanei, C. briggsae* and *C. japonica* near the *lin-4* locus and promoters used in the expression analysis. Green bars indicate H3K4me3 ChIP-seq data tracks (indicative of active promoters near transcriptional start sites). Black bars indicate the localization of open chromatin as measured from ATAC-seq experiments.[28]

(B) Representative measurements of full-length *lin-4::GFP-pest* expression levels in lateral seam cells. The fluorescent intensity of five seam cells per animal were averaged and 8-15 animals were measured per indicated L4 morphological substage.

(C) Representative fluorescence and DIC images of the full-length *lin-4::GFP-pest* transcriptional reporter in the hypodermal cells of developing L4-staged animals. L4-stage numbers correspond to the defined sub-stages of vulval morphological development (Sn = seam cell nuclei, h = hyp7 cell nuclei, and m = muscle cell nuclei).[30]

(D) Measurements of seam cell expression levels for the various *lin-4::GFP-pest* reporter constructs outlined in panel A at the L4.5 stage of development. (n= 5-10 animals per transgenic strain)

(E) Representative images of each transcriptional reporter outlined in D. Individual labels defining cell types are the same as in panel C.

(F) Position Weight Matrix of the consensus BLMP-1 binding site calculated from ChIP-seq data outlined in Figure 3A and two sequences located in the minCE element that conform to this consensus.

(G) Gel shift experiments demonstrating that a GST fusion protein harboring the 5 ZnF domains of BLMP-1 (but not GST alone) can bind to the two sequences outlined in panel F.

(H) Comparison of the GFP-pest expression patterns of *gst-5::GFP-pest* or *(2xminCE)gst-5::GFP*-pest in late L1-stage animals. The pulsatile expression of the *(2xminCE)gst-5::GFP*-pest expression correlates with a single pulse in the middle of each larval stage. For the developmental time course, a minimum of forty animals expressing *gst-5::GFP-pest* or *(2xminCE)gst-5::GFP*-pest were scored. See also Figure S2 and S4.

Figure 5. *blmp-1* modulates the amplitude and transcriptional duration of their cyclically expressed targets. (A-C) Quantification of GFP-pest expression from the *(2xminCE)gst-5*, *C02E7.6* and *moe-3* transcriptional reporters in L4-staged animals. Top panel for each reporter

indicates the average fluorescent intensity of GFP-pest expression in the lateral seam cells for each morphologically defined L4 stage ((*2xminCE)gst-5* = L4.5, C02E7.6 = L4.5, and *moe-3* = L4.9) (n = 7-14 animals)(Sn = seam cell nuclei).

(D) Merged DIC and fluorescence micrographs (after worm axis straightening[31]) showing reporter expression at peak intensity in the L2 stage.

(E) Estimation plot[70] showing the duration of second larval stage (L2) for WT (N=92), *blmp-1(0)* (N=46), *elt-3(0)* (N=15) and *blmp-1(0); elt-3(0)* animals (N=50). Upper row: Grey circles indicate L2 duration, measured by observing cuticle shedding (molts) during long-term live imaging using a microfluidics device (Keil et al., 2016). (see Methods). Black error bars indicate mean and standard deviation. Lower row: Mean bootstrapped difference values compared to WT and 95% confidence intervals of bootstrap distributions (black error bars). See also Figure S5.

(F) *ZK180.5*::*GFP-pest* reporter intensity, averaged over the entire animal throughout development as a function of time for WT (light red, N=23, dark red average) and *blmp-1(0)* mutant (light blue, N=13, dark blue average). Time courses are scaled such that molts (dashed grey lines) of individual animals align with average WT molting timings.

(G) Inset of (F), showing the fluorescence intensity during the L2 stage of development.

(H) L2 peak fluorescence intensity (left most), onset phase of reporter expression (left middle), peak phase of reporter expression (right middle) and Output (AOC = area under the curve) (right most) for the *ZK180.5*::*GFP-pest* reporter in WT (red circles, N=21) and *blmp-1(0)* mutant (blue circles, N=13). Black triangles indicate mean bootstrapped difference values, blue error bars indicate 95% confidence intervals of bootstrapped difference distribution. See also Figure S6.

(I,J) As (F, G) but for *mlt-10*::*GFP-pest* (WT, N=7; *blmp-1(0)*, N=5*).* See also Figure S6.

Figure 6. The *lin-4* locus is maintained in an open chromatin state in hypodermal cells in a *blmp-1*-dependent manner.

(A) Schematic of the transgenic array used for visualization of the *lin-4* locus in living animals.

(B) Representative image of L1-staged animals expressing the GFP-lacO-labeled *lin-4* locus.

(C) Analysis of the expression pattern of an endogenously GFP-tagged translational fusion of BLMP-1 indicating that expression begins in hypodermal cells around the bean stages and remains stably expressed throughout embryonic development.

(D) Pictographs depicting the compression level of the *lin-4* locus/GFP-LacI foci in differentially staged wild-type and *blmp-1(0)* mutant embryos. Yellow arrows indicate the location of hypodermal nuclei.

(E) Quantification of the percentage of wild-type or *blmp-1(0)* late-stage (pretzel) embryos that exhibit decompacted *lin-4* loci in hypodermal cells.

(F) Close-up images of representative seam cell and neuronal nuclei from L3-staged wild-type and *blmp-1(0)* mutant larva. GFP images are the maximum intensity projections obtained for each relevant nuclei.

(G) Quantification of the sizes of the nuclear GFP-LacI foci in various cell types of wild-type and *blmp-1(0)* mutant animals. For each cell type, GFP-LacI areas were quantified from greater than 18 individual nuclei from each genotype. Boxes and median line indicate the interquartile range. Whiskers cover 10-90th percentile. Circles represent outliers. Brackets indicate statistically significant differences in "puffs size" calculated from a two-tailed chi-square analysis.

Figure 7. Dynamic gene expression is halted during nutrition-mediated developmental arrest and BLMP-1 and ELT-3 are essential for the recovery of normal temporal patterning after starvation.

(A) A schematic of the starvation experiment used to measure nutrient-depended changes in the expression patterns of cyclically expressed genes. See also Figure S7.

(B) Continuous cycling of gene expression is arrested during starvation conditions and is reinitiated in a coordinated manner when animals resume development. For each timepoint, 70-200 animals were scored.

(C) BLMP-1::GFP expression is down-regulated during starvation conditions and expression is rapidly resumed when animals reinitiate development. See also Figure S7 for L1 starvation data.

(D) The *lin-4* locus is compacted during starvation conditions in lateral seam cells. Data for each condition was quantified as in Figure 6G. See also Figure S7

(E) A schematic of the starvation-mediated arrest and re-feeding experiment used to measure the ability of animals to resume normal temporal patterning after starvation.

(F) The resumption of normal temporal patterning after starvation requires *blmp-1* and *elt-3* activity. Defects in temporal development were monitored by measuring the *col-19::GFP* expression phenotypes in re-fed animals after they resumed growth for 24hours after the indicated period of starvation. (n = >100 per condition)

892 **(G)** Representative pictographs of the *col-19::GFP* phenotypes in wild-type and *blmp-1(0); elt-*
893 *3(0)* mutants after animals have recovered from 5 days of starvation.
894 **(H)** A diagram outlining the expression features of a single transcriptional cycle in wild-type and
895 *blmp-1(0)* animals.
896 **(I)** A model for how BLMP-1 and ELT-3 function to regulate transcriptional output during larval
897 development.
898 **(J)** A diagram outlining the changes of *blmp-1* mRNA and BLMP-1 protein levels during normal
899 grown and during starvation conditions.
900

STAR METHODS

LEAD CONTACT AND MATERIALS AVAILABILITY

Further information and requests for resources and reagents should be directed to and will be fulfilled by the Lead Contact, Christopher M. Hammell (chammell@cshl.edu). Plasmids generated in this study are available upon request made to the Lead Contact. *C. elegans* strains generated in this study are available upon request made to the Lead Contact.

Data and Code Availability

A public repository containing MATLAB scripts used for figures and statistical analyses in this paper can be found at https://github.com/wolfgangkeil/Stec_et_al_2020_code.

EXPERIMENTAL MODEL AND SUBJECT DETAILS

C. elegans maintenance and genetics

C. elegans strains were maintained on standard media at 20°C and fed *E. coli* OP50.[71] A list of strains used in this study is provided in the Key Resources Table. Some strains were provided by the CGC, which is funded by NIH Office of Research Infrastructure Programs (P40 OD010440). *blmp-1(tm548)* was obtained from Shohei Mitani the National BioResource Project (NBRP) at the Tokyo Women's Medical University.

METHOD DETAILS

RNAi feeding

RNAi by feeding was performed using E. coli HT115 expressing double stranded RNA corresponding to *blmp-1* or *elt-3*, or containing a control dsRNA expression plasmid that does not contain sequence corresponding to any *C. elegans* gene.[72,73] To prevent contamination by *E. coli* OP50, gravid adult animals were added to RNAi plates individually after removing co-transferred bacteria. Unless otherwise noted, F1 progeny were analyzed for RNAi-induced phenotypes following 2-4 days.

Transgenesis

Cloning was performed using the Gibson Assembly Master Mix (New England Biolabs, #E2611L). Extra-chromosomal arrays were generated using *ttx-3::GFP* as a co-injection

marker and *unc-119* rescue to select transformants. Gamma ray mutagenesis was used to induce integration of extrachromosomal arrays.[74]

GFP tagged alleles of *blmp-1*

We amplified two 0.5kb-long homology arms from N2 genomic DNA flanking the *blmp-1* gene and the GFP open reading frame using standard PCR. These fragments were used with Gibson cloning to insert them into a pMCS5 backbone. The resulting plasmid, pCMH1406, was used in combination with pCMH1410 and standard protocols[75] to integrate GFP at the *blmp-1* locus. The resulting animals were characterized phenotypically for alae defects that are associated with *blmp-1(0)*. The GFP-tagged allele was wild type.

Microscopy

Images were acquired with a Zeiss Axio Observer microscope equipped with Nomarski and fluorescence optics as well as a Hamamatsu Orca Flash 4.0 FL Plus camera. An LED lamp emitting at 470 nm was used for fluorophore excitation. For single images, animals were immobilized on 2% agarose pads supplemented with 100mM Levamisole (Sigma). For long-term imaging methods, see Microfluidics and Long-term Imaging section.

Chromatin immunoprecipitation

BLMP-1 short reads were first clipped off adapter sequences. Reads of minimum 22bp were mapped to UCSC *C. elegans* genome (ce10) using bowtie program[76], looking for unique alignments with no more than 2 mismatches. MACS program (v1.4)[77] was used for peak calling with significant p-value cutoff equals 1e-5. Target annotations were based on WormBase (version 220) using customized R scripts and Bioconductor packages. We defined the promoter region as upstream 3kbp to downstream 300bp around transcription start site (TSS). Peaks located in promoter regions were annotated to their closest TSS sites for both coding and non-coding genes. These potential targets were then overlapped to sets of oscillatory genes identified in previous mRNA-seq-based studies[7,8] and the two-tailed Fisher's test was used to calculate the p-values associated with these classifications. ELT-3 (Embryo and L1-staged) raw data were downloaded from modENCODE and processed in the same way as BLMP-1. Peaks from each CHiP-seq dataset were compared to identify common sites with

at least one base pair overlapping using BEDTools.[78] All ChIP-seq mapping graphs and images were produced in R by customized scripts.

Microfluidics and long-term imaging

For microfluidics experiments, early to mid L1-staged animals were isolated through a 1-2 hours timed egg-lay approximately 12-14 hours at 20°C before an experimental time course. Animals were mounted into the microfluidic device as previously described.[31] During the imaging process, animals were constantly fed NA22 *E. coli* suspended in S medium. Imaging was done with a 40x, 1.3NA objective using an Andor Zyla 4.2 scMOS camera. The temperature was kept constant at 20˚C both, at the objective and the microfluidic device using a custom-built water-cooled aluminum ring (for objective) and custom-built aluminum stage inset that was directly coupled to a thermal Peltier device.[31]

Native gel shifts

For recombinant GST-BLMP-1(ZnFs) protein expression, an approximately 400bp PCR fragment (with BamHI ends) was subcloned into the BamHI sites of pGex-3X. The resulting plasmid, pCMH1417, or pGEX-3X alone, was transformed into BLM21(DE3) E. coli. Cultures of these bacteria were grown to an O.D. of 0.5 A600 in LB+amp and induced with 0.2mM IPTG for 2 hours at 37°C. Cell pellets were resuspended in PBS and then sonicated and clarified by centrifugation. Fusion proteins were isolated on glutathione-agarose and eluted with glutathione. The resulting fusion proteins were then dialyzed in 10 mM Tris 7.5, 50 mM NaCl, 0.01% NP-40 1 mM DTT overnight and snap frozen in liquid nitrogen. For gel shifts with free DNA, 5' IRDye (IRDye700 or IRDye800)-labeled and unlabeled oligos were obtained from IDT (Coralville, Iowa). The sequences of these oligos are the following:

lin-4 site 1 sequence (+) CTTTCTCCTTCACTTTCTCTCTCTCGGATCACCAG
lin-4 site 1 sequence (-) CTGGTGATCCGAGAGAGAGAAAGTGAAGGAGAAAG
lin-4 site 2 sequence (+) ATGGGAAAATAGAAAGAGAAAATGAGAGAAAGGAT
lin-4 site 2 sequence (-) CTTTCTCTCATTTTCTCTTTCTATTTTCCCAT
non-specific sequence (+) GGCTCTTCCGGTCGTGCAAGAGGAAATACAAAAAA
non-specific sequence (-) TTTTTTGTATTTCCTCTTGCACGACCGGAAGAGCC

Complementary oligos were annealed in TE to a final concentration of 0.1 pmol/µL. 0.1 pmol of these probes were incubated with recombinant GST or GST-BLMP-1(ZnFs) in 10 mM Tris pH 7.5, 50 mM KCl, 1 mM DTT, 0.1µg/µL poly (dIdC) 0.25% Tween 20 for 30 minutes at 20°C (in dark chamber) and then run in a 4% native polyacrylamide gel containing 50mM Tris

pH 7.5, 0.38 M glycine and 2mM EDTA in 1x TBE buffer. Gels were imaged using a Licor Odyssey Imager (Lincoln, Nebraska).

Chromatin decompaction assays

To analyze the compaction state of the *lin-4* locus, we exploited the LacI/LacO approach as previously described.[37] The arrays containing *lin-4* were generated by co-injecting the following components: a) 2ng/µL of linearized pIF9 (*unc-119(+)*), b) 3ng/µL of linearized pCMH1972 (256x LacO sites), 3ng/µL of pCMH1984 (*lin-4pro::SL2::mCherry-pest*), and 90ng/µL of sheared salmon sperm DNA (Invitrogen). Transgenic lines produced in this manner (e.g. *cshIs116*) were integrated using standard procedures and outcrossed into a strain harboring *otIs593* (*ttx-3::mCherry; let-858pro::GFP::LacI*)(Gift of O. Hobert). For imaging nuclear spots assay of either eggs or staged L3/L4 molt animals, Z-stacks (0.3µm spacing) were collected using three channels: DIC, GFP (150ms exposure) and mCherry (60ms exposure). Both acquisition and post-acquisition processing was performed using ZEN Pro software (Zeiss). Maximum-intensity projections of the planes that span the nuclei of interest were obtained separately for seam and head area. The projections were then exported to Fiji[79] and manual traces of areas of the nuclei with GFP intensity above background were made to measure locus compaction/decompaction as described.[33]

Food removal assays

Starvation experiments were performed as previously described.[47] Briefly, embryos were isolated from gravid adult animals using a standard, hypochlorite treatments and allowed to hatch in M9 buffer. L1 staged/arrested animals were plated onto NGM plates seeded with OP50 *E. coli* at a concentration lower that 2,500 animals per 60 mm petri dish. Animals were then grown for the indicated amount of time at 20°C unless otherwise noted. Assessment of developmental age was made by direct observation of gonad growth or by specific cell lineage landmarks of lateral seam cells or developing vulval precursor cells. Acute starvation was induced by washing animals off the petri dishes and washing them with M9 for nine times. After the final was animals were resuspended in M9 buffer to a concentration of ~1 animal per µL of sterile M9. Animals were maintained in these starvation conditions at 20°C for the indicated times. Animal development was re-initiated by plating animals onto fresh OP50 *E. coli*-seeded NGM plates at 20°C.

Quantification Of Gene Expression using GFP reporters

Fluorescence intensities were quantified using ImageJ custom-written MATLAB scripts. software. For measurement of reporter gene expression for time course experiments, we performed dual channel imaging, visualizing gene expression patterns by visualizing GFP-pest expression and overall worm morphology with Nomarski microscopy (DIC). We straightened each three-dimensional image stack using a previously published algorithm[31] based on a worm backbone which was manually outlined using the DIC channel. The resulting straightened worm z-stacks were then cropped in xy to a region of interest. To deconvolve the straightened, cropped *GFP-pest* reporter z stacks, we measured the point-spread function (PSF) of our optical setup using red (580/605nm) fluorescent 200nm beads (ThermoFisher Scientific). Using the obtained PSFs, we deconvolved stacks using the classic maximum likelihood estimation (CMLE) algorithm with standard parameters (refractive index of imaging medium: 1.338) in the Huygens Essential software (Huygens Essential 3.7.1) by Scientific Volume Imaging (SVI).

Statistical Analysis

All statistical analyses were performed in MATLAB or GraphPad Prism 9, either using built-in functions (chi squared, Student's t tests) or custom-written scripts (bootstrap permutation test). Differences between two groups are judged to be statistically significant when $p < 0.05$ by Student's t test or bootstrap permutation test, where appropriate. Mean and SEM were calculated and plotted using GraphPad Prism or custom scripts. T-tests analyses are based on the normal distribution theory. We did not test the assumption of normality because even when the raw data are not exactly normally distributed, these analysis methods are very robust to departures from normality as long as the sample sizes are larger than approximately 30. For Figure 3, changes in translational reporter expression for BLMP-1::GFP and ELT-3::GFP were quantified as previously described. [31] Each circle in panel F represents the average GFP fluorescence for 3 hypodermal cells per animal for each translational reporter. For Figure 4, n = number of animals scored in each assay. GraphPad Prism software was used to calculate Mean expression level for each time point measured. Each circle represents the average GFP fluorescence for 3 seam cells per animal. For Figure 5, GraphPad Prism software was used to calculate Mean expression levels. For A-C, each circle represents the average GFP fluorescence for 3 seam cells per animal. For E, each circle represents the duration from one

ecdysis event to the next in the L1 to L2 molt cycle. Image analysis was performed as in Keli et al. 2016.[31] Estimation plots were calculated as previously describted.[70] For Figure 6, panel E, n = number of animals scored in each assay. For Panel G, GFP-LacI areas were quantified from greater that 18 individual nuclei from separate animals for each genotype. GraphPad Prism software was used to plot image data and box plots show data within the 10-90th percentile with whiskers. For Figure 7, n = number of animals scored in each assay. GraphPad Prism software was used to calculate Mean. For panel D, GFP-LacI areas were quantified from greater than 20 seam cell nuclei from separate animals in each condition.

Data S1. Summary of ChIP-seq experiments for BLMP-1::GFP and ELT-3::GFP, related to Figure 3. Tables include gene assignments for L1-L4 BLMP-1 (Data S1A-D) and L1 ELT-3 ChIP-seq data sets (Data S1E).

Data S2. Comparison of ChIP-seq data to mRNA expression classes as defined by Hendriks et al.[8] and Kim et al.[7] time course data sets, related to Figure 3. Tables include gene class assignments (flat, oscillating and rising) of ModEncode ChIP-seq data (Data S2A) and assignments of BLMP-1 ChIP-seq data sets to expression cluster data (Data S2B).

REFERENCES

1 Ambros, V. & Horvitz, H. R. Heterochronic mutants of the nematode Caenorhabditis elegans. *Science* 226, 409-416 (1984).

2 Rougvie, A. E. & Moss, E. G. Developmental Transitions in *C. elegans* Larval Stages. *Curr Top Dev Biol* 105, 153-180, doi:10.1016/B978-0-12-396968-2.00006-3 (2013).

3 Feinbaum, R. & Ambros, V. The timing of lin-4 RNA accumulation controls the timing of postembryonic developmental events in Caenorhabditis elegans. *Developmental biology* 210, 87-95. (1999).

4 Li, M., Jones-Rhoades, M. W., Lau, N. C., Bartel, D. P. & Rougvie, A. E. Regulatory mutations of mir-48, a *C. elegans let-7* family MicroRNA, cause developmental timing defects. *Developmental cell* 9, 415-422, doi:10.1016/j.devcel.2005.08.002 (2005).

5 Perales, R., King, D. M., Aguirre-Chen, C. & Hammell, C. M. LIN-42, the *Caenorhabditis elegans* PERIOD homolog, Negatively Regulates MicroRNA Transcription. *PLoS genetics* 10, e1004486, doi:10.1371/journal.pgen.1004486 (2014).

6 Van Wynsberghe, P. M. & Pasquinelli, A. E. Period homolog LIN-42 regulates miRNA transcription to impact developmental timing. *Worm* 3, e974453, doi:10.4161/21624054.2014.974453 (2014).

7 Kim, D. h., Grün, D. & van Oudenaarden, A. Dampening of expression oscillations by synchronous regulation of a microRNA and its target. *Nat Genet* 45, 1337-1344, doi:10.1038/ng.2763 (2013).

8 Hendriks, G.-J., Gaidatzis, D., Aeschimann, F. & Großhans, H. Extensive Oscillatory Gene Expression during *C. elegans* Larval Development. *Mol Cell* 53, 380-392, doi:10.1016/j.molcel.2013.12.013 (2014).

9 Hurley, J. M., Loros, J. J. & Dunlap, J. C. Circadian Oscillators: Around the Transcription-Translation Feedback Loop and on to Output. *Trends Biochem Sci* 41, 834-846, doi:10.1016/j.tibs.2016.07.009 (2016).

10 Jeon, M., Gardner, H. F., Miller, E. A., Deshler, J. & Rougvie, A. E. Similarity of the *C. elegans* developmental timing protein LIN-42 to circadian rhythm proteins. *Science* 286, 1141-1146 (1999).

11 Monsalve, G. C., Van Buskirk, C. & Frand, A. R. LIN-42/PERIOD controls cyclical and developmental progression of *C. elegans* molts. *Current biology : CB* 21, 2033-2045, doi:10.1016/j.cub.2011.10.054 (2011).

12 McCulloch, K. A. & Rougvie, A. E. Caenorhabditis elegans period homolog lin-42 regulates the timing of heterochronic miRNA expression. *Proceedings of the National Academy of Sciences of the United States of America* 111, 15450-15455, doi:10.1073/pnas.1414856111 (2014).

13 Tennessen, J. M., Opperman, K. J. & Rougvie, A. E. The *C. elegans* developmental timing protein LIN-42 regulates diapause in response to environmental cues. *Development* 137, 3501-3511, doi:10.1242/dev.048850 (2010).

14 Abrahante, J. E., Miller, E. A. & Rougvie, A. E. Identification of heterochronic mutants in *Caenorhabditis elegans*. Temporal misexpression of a

collagen::green fluorescent protein fusion gene. *Genetics* 149, 1335-1351 (1998).
15 Cao, J. *et al.* Comprehensive single-cell transcriptional profiling of a multicellular organism. *Science* 357, 661-667, doi:10.1126/science.aam8940 (2017).
16 Horn, M. *et al.* DRE-1/FBXO11-Dependent Degradation of BLMP-1/BLIMP-1 Governs *C. elegans* Developmental Timing and Maturation. *Developmental cell*, doi:10.1016/j.devcel.2014.01.028 (2014).
17 Hammell, C. M., Lubin, I., Boag, P. R., Blackwell, T. K. & Ambros, V. nhl-2 Modulates microRNA activity in *Caenorhabditis elegans*. *Cell* 136, 926-938 (2009).
18 Sulston, J. E. & Horvitz, H. R. Post-embryonic cell lineages of the nematode, *Caenorhabditis elegans*. *Developmental biology* 56, 110-156. (1977).
19 Tuck, S. The control of cell growth and body size in *Caenorhabditis elegans*. *Experimental cell research* 321, 71-76, doi:10.1016/j.yexcr.2013.11.007 (2014).
20 Hayes, G. D., Frand, A. R. & Ruvkun, G. The mir-84 and let-7 paralogous microRNA genes of *Caenorhabditis elegans* direct the cessation of molting via the conserved nuclear hormone receptors NHR-23 and NHR-25. *Development* 133, 4631-4641, doi:10.1242/dev.02655 (2006).
21 Frand, A. R., Russel, S. & Ruvkun, G. Functional genomic analysis of *C. elegans* molting. *PLoS biology* 3, e312, doi:10.1371/journal.pbio.0030312 (2005).
22 Beitel, G. J., Clark, S. G. & Horvitz, H. R. *Caenorhabditis elegans* ras gene let-60 acts as a switch in the pathway of vulval induction. *Nature* 348, 503-509 (1990).
23 Han, M. & Sternberg, P. W. let-60, a gene that specifies cell fates during *C. elegans* vulval induction, encodes a ras protein. *Cell* 63, 921-931 (1990).
24 Araya, C. L. *et al.* Regulatory analysis of the *C. elegans* genome with spatiotemporal resolution. *Nature* 512, 400-405, doi:10.1038/nature13497 (2014).
25 Niu, W. *et al.* Diverse transcription factor binding features revealed by genome-wide ChIP-seq in *C. elegans. Genome research* 21, 245-254, doi:10.1101/gr.114587.110 (2011).
26 Lee, R. C., Feinbaum, R. L. & Ambros, V. The *C. elegans* heterochronic gene *lin-4* encodes small RNAs with antisense complementarity to lin-14. *Cell* 75, 843-854. (1993).
27 Bracht, J. R., Van Wynsberghe, P. M., Mondol, V. & Pasquinelli, A. E. Regulation of lin-4 miRNA expression, organismal growth and development by a conserved RNA binding protein in *C. elegans*. *Developmental biology* 348, 210-221, doi:10.1016/j.ydbio.2010.10.003 (2010).
28 Daugherty, A. C. *et al.* Chromatin accessibility dynamics reveal novel functional enhancers in *C. elegans. Genome research* 27, 2096-2107, doi:10.1101/gr.226233.117 (2017).
29 Janes, J. *et al.* Chromatin accessibility dynamics across *C. elegans* development and ageing. *Elife* 7, doi:10.7554/eLife.37344 (2018).

30 Mok, D. Z. L., Sternberg, P. W. & Inoue, T. Morphologically defined sub-stages of *C. elegans* vulval development in the fourth larval stage. *BMC developmental biology* 15, 26, doi:10.1186/s12861-015-0076-7 (2015).
31 Keil, W., Kutscher, L. M., Shaham, S. & Siggia, E. D. Long-Term High-Resolution Imaging of Developing *C. elegans* Larvae with Microfluidics. *Developmental cell*, doi:10.1016/j.devcel.2016.11.022 (2016).
32 Fong, H. T., Hagen, T. & Inoue, T. LDB1 and the SWI/SNF complex participate in both transcriptional activation and repression by *Caenorhabditis elegans* BLIMP1/PRDM1. *Biochim Biophys Acta Gene Regul Mech* 1863, 194577, doi:10.1016/j.bbagrm.2020.194577 (2020).
33 Cochella, L. & Hobert, O. Embryonic priming of a miRNA locus predetermines postmitotic neuronal left/right asymmetry in *C. elegans*. *Cell* 151, 1229-1242, doi:10.1016/j.cell.2012.10.049 (2012).
34 Hsu, H.-T. *et al.* TRANSCRIPTION. Recruitment of RNA polymerase II by the pioneer transcription factor PHA-4. *Science* 348, 1372-1376, doi:10.1126/science.aab1223 (2015).
35 Patel, T. & Hobert, O. Coordinated control of terminal differentiation and restriction of cellular plasticity. *eLife* 6, 249, doi:10.7554/eLife.24100 (2017).
36 Fakhouri, T. H., Stevenson, J., Chisholm, A. D. & Mango, S. E. Dynamic chromatin organization during foregut development mediated by the organ selector gene PHA-4/FoxA. *PLoS Genet* 6, doi:10.1371/journal.pgen.1001060 (2010).
37 Meister, P., Towbin, B. D., Pike, B. L., Ponti, A. & Gasser, S. M. The spatial dynamics of tissue-specific promoters during *C. elegans* development. *Genes & development* 24, 766-782, doi:10.1101/gad.559610 (2010).
38 Dietzel, S., Zolghadr, K., Hepperger, C. & Belmont, A. S. Differential large-scale chromatin compaction and intranuclear positioning of transcribed versus non-transcribed transgene arrays containing beta-globin regulatory sequences. *J Cell Sci* 117, 4603-4614, doi:10.1242/jcs.01330 (2004).
39 Tumbar, T., Sudlow, G. & Belmont, A. S. Large-scale chromatin unfolding and remodeling induced by VP16 acidic activation domain. *J Cell Biol* 145, 1341-1354, doi:10.1083/jcb.145.7.1341 (1999).
40 Yuzyuk, T., Fakhouri, T. H., Kiefer, J. & Mango, S. E. The polycomb complex protein mes-2/E(z) promotes the transition from developmental plasticity to differentiation in *C. elegans* embryos. *Dev Cell* 16, 699-710, doi:10.1016/j.devcel.2009.03.008 (2009).
41 Mutlu, B. *et al.* Distinct functions and temporal regulation of methylated histone H3 during early embryogenesis. *Development* 146, doi:10.1242/dev.174516 (2019).
42 Mutlu, B. *et al.* Regulated nuclear accumulation of a histone methyltransferase times the onset of heterochromatin formation in *C. elegans* embryos. *Sci Adv* 4, eaat6224, doi:10.1126/sciadv.aat6224 (2018).
43 Towbin, B. D. *et al.* Step-wise methylation of histone H3K9 positions heterochromatin at the nuclear periphery. *Cell* 150, 934-947, doi:10.1016/j.cell.2012.06.051 (2012).

44 Ow, M. C. *et al.* The FLYWCH transcription factors FLH-1, FLH-2, and FLH-3 repress embryonic expression of microRNA genes in *C. elegans*. *Genes & development* 22, 2520-2534 (2008).
45 Hedgecock, E. M. & White, J. G. Polyploid tissues in the nematode *Caenorhabditis elegans. Dev Biol* 107, 128-133, doi:10.1016/0012-1606(85)90381-1 (1985).
46 Frezal, L. & Felix, M. A. C. elegans outside the Petri dish. *Elife* 4, doi:10.7554/eLife.05849 (2015).
47 Schindler, A. J., Baugh, L. R. & Sherwood, D. R. Identification of late larval stage developmental checkpoints in *Caenorhabditis elegans* regulated by insulin/IGF and steroid hormone signaling pathways. *PLoS genetics* 10, e1004426, doi:10.1371/journal.pgen.1004426 (2014).
48 Abbott, A. L. *et al.* The let-7 MicroRNA family members mir-48, mir-84, and mir-241 function together to regulate developmental timing in *Caenorhabditis elegans. Developmental cell* 9, 403-414 (2005).
49 Hasty, J., Hoffmann, A. & Golden, S. Systems biology of cellular rhythms: from cacophony to symphony. *Curr Opin Genet Dev* 20, 571-573, doi:10.1016/j.gde.2010.10.003 (2010).
50 Shigeyoshi, Y. *et al.* Light-induced resetting of a mammalian circadian clock is associated with rapid induction of the mPer1 transcript. *Cell* 91, 1043-1053, doi:10.1016/s0092-8674(00)80494-8 (1997).
51 Trott, A. J. & Menet, J. S. Regulation of circadian clock transcriptional output by CLOCK:BMAL1. *PLoS Genet* 14, e1007156, doi:10.1371/journal.pgen.1007156 (2018).
52 Moreno-Risueno, M. A. *et al.* Oscillating gene expression determines competence for periodic Arabidopsis root branching. *Science* 329, 1306-1311, doi:10.1126/science.1191937 (2010).
53 Kircher, S. & Schopfer, P. Priming and positioning of lateral roots in Arabidopsis. An approach for an integrating concept. *J Exp Bot* 67, 1411-1420, doi:10.1093/jxb/erv541 (2016).
54 Bao, Y. *et al.* Plant roots use a patterning mechanism to position lateral root branches toward available water. *Proc Natl Acad Sci U S A* 111, 9319-9324, doi:10.1073/pnas.1400966111 (2014).
55 Meeuse, M. W. *et al.* Developmental function and state transitions of a gene expression oscillator in *Caenorhabditis elegans. Mol Syst Biol* 16, e9498, doi:10.15252/msb.20209498 (2020).
56 Ambros, V. MicroRNAs and developmental timing. *Current opinion in genetics & development* 21, 511-517, doi:10.1016/j.gde.2011.04.003 (2011).
57 Minnich, M. *et al.* Multifunctional role of the transcription factor Blimp-1 in coordinating plasma cell differentiation. *Nat Immunol* 17, 331-343, doi:10.1038/ni.3349 (2016).
58 Liang, H. L. *et al.* The zinc-finger protein Zelda is a key activator of the early zygotic genome in Drosophila. *Nature* 456, 400-403, doi:10.1038/nature07388 (2008).
59 Foo, S. M. *et al.* Zelda potentiates morphogen activity by increasing chromatin accessibility. *Curr Biol* 24, 1341-1346, doi:10.1016/j.cub.2014.04.032 (2014).

60 McDaniel, S. L. *et al.* Continued Activity of the Pioneer Factor Zelda Is Required to Drive Zygotic Genome Activation. *Mol Cell* 74, 185-195 e184, doi:10.1016/j.molcel.2019.01.014 (2019).
61 Rushlow, C. A., Han, K., Manley, J. L. & Levine, M. The graded distribution of the dorsal morphogen is initiated by selective nuclear transport in Drosophila. *Cell* 59, 1165-1177, doi:10.1016/0092-8674(89)90772-1 (1989).
62 Roth, S., Stein, D. & Nusslein-Volhard, C. A gradient of nuclear localization of the dorsal protein determines dorsoventral pattern in the Drosophila embryo. *Cell* 59, 1189-1202, doi:10.1016/0092-8674(89)90774-5 (1989).
63 Yamada, S. *et al.* The Drosophila Pioneer Factor Zelda Modulates the Nuclear Microenvironment of a Dorsal Target Enhancer to Potentiate Transcriptional Output. *Curr Biol* 29, 1387-1393 e1385, doi:10.1016/j.cub.2019.03.019 (2019).
64 Evertts, A. G. *et al.* H4K20 methylation regulates quiescence and chromatin compaction. *Mol Biol Cell* 24, 3025-3037, doi:10.1091/mbc.E12-07-0529 (2013).
65 Laporte, D., Courtout, F., Tollis, S. & Sagot, I. Quiescent Saccharomyces cerevisiae forms telomere hyperclusters at the nuclear membrane vicinity through a multifaceted mechanism involving Esc1, the Sir complex, and chromatin condensation. *Mol Biol Cell* 27, 1875-1884, doi:10.1091/mbc.E16-01-0069 (2016).
66 Pinon, R. Folded chromosomes in non-cycling yeast cells: evidence for a characteristic g0 form. *Chromosoma* 67, 263-274, doi:10.1007/BF02569039 (1978).
67 Rawlings, J. S., Gatzka, M., Thomas, P. G. & Ihle, J. N. Chromatin condensation via the condensin II complex is required for peripheral T-cell quiescence. *EMBO J* 30, 263-276, doi:10.1038/emboj.2010.314 (2011).
68 Rutledge, M. T., Russo, M., Belton, J. M., Dekker, J. & Broach, J. R. The yeast genome undergoes significant topological reorganization in quiescence. *Nucleic Acids Res* 43, 8299-8313, doi:10.1093/nar/gkv723 (2015).
69 Swygert, S. G. *et al.* Condensin-Dependent Chromatin Compaction Represses Transcription Globally during Quiescence. *Mol Cell* 73, 533-546 e534, doi:10.1016/j.molcel.2018.11.020 (2019).
70 Ho, J., Tumkaya, T., Aryal, S., Choi, H. & Claridge-Chang, A. Moving beyond P values: data analysis with estimation graphics. *Nat Methods* 16, 565-566, doi:10.1038/s41592-019-0470-3 (2019).
71 Brenner, S. The genetics of *Caenorhabditis elegans. Genetics* 77, 71-94 (1974).
72 Fraser, A. G. *et al.* Functional genomic analysis of C. elegans chromosome I by systematic RNA interference. *Nature* 408, 325-330. (2000).
73 Kamath, R. S. *et al.* Systematic functional analysis of the *Caenorhabditis elegans g*enome using RNAi. *Nature* 421, 231-237 (2003).
74 Mello, C. C., Kramer, J. M., Stinchcomb, D. & Ambros, V. Efficient gene transfer in C.elegans: extrachromosomal maintenance and integration of transforming sequences. *The EMBO journal* 10, 3959-3970 (1991).
75 Dickinson, D. J., Ward, J. D., Reiner, D. J. & Goldstein, B. Engineering the *Caenorhabditis elegans* genome using Cas9-triggered homologous recombination. *Nature methods* 10, 1028-1034, doi:10.1038/nmeth.2641 (2013).

76 Langmead, B., Trapnell, C., Pop, M. & Salzberg, S. L. Ultrafast and memory-efficient alignment of short DNA sequences to the human genome. *Genome biology* 10, R25, doi:10.1186/gb-2009-10-3-r25 (2009).
77 Zhang, Y. *et al.* Model-based analysis of ChIP-Seq (MACS). *Genome biology* 9, R137-139, doi:10.1186/gb-2008-9-9-r137 (2008).
78 Quinlan, A. R. & Hall, I. M. BEDTools: a flexible suite of utilities for comparing genomic features. *Bioinformatics* 26, 841-842, doi:10.1093/bioinformatics/btq033 (2010).
79 Schindelin, J. *et al.* Fiji: an open-source platform for biological-image analysis. *Nature methods* 9, 676-682, doi:10.1038/nmeth.2019 (2012).

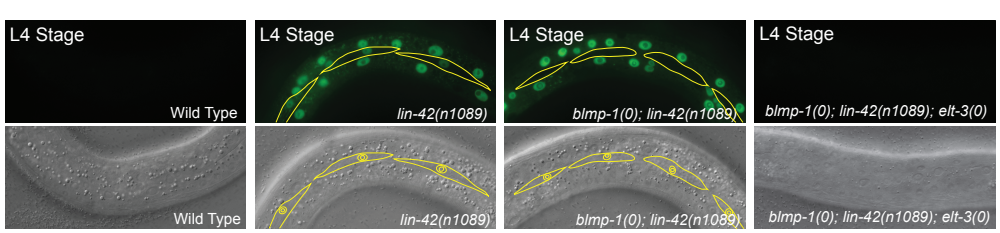

B

	L4 Stage			n =	Adult Stage		n =
Wild Type	100 %	0 %	0 %	35	0 %	100 %	100
lin-42(n1089)	8 %	0 %	92 %	25	0 %	100 %	100
blmp-1(0)	100 %	0 %	0 %	35	1 %	99 %	182
elt-3(0)	100 %	0 %	0 %	35	0 %	100 %	101
blmp-1(0); elt-3(0)	100 %	0 %	0 %	39	5 %	95 %	88
blmp-1(0); lin-42(n1089)	28 %	72 %	0 %	25	0 %	100 %	100
lin-42(n1089); elt-3(0)	8 %	21 %	71 %	28	0 %	100 %	100
blmp-1(0); lin-42(n1089); elt-3(0)	65 %	35 %	0 %	34	0 %	100 %	100

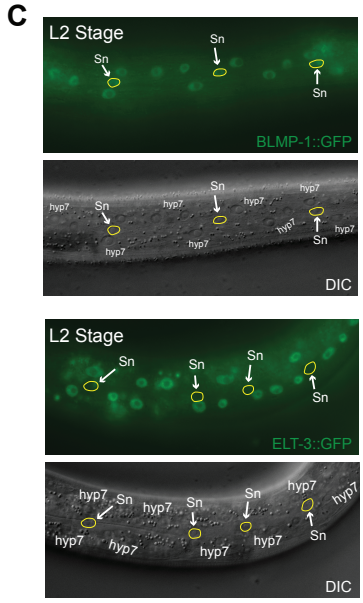

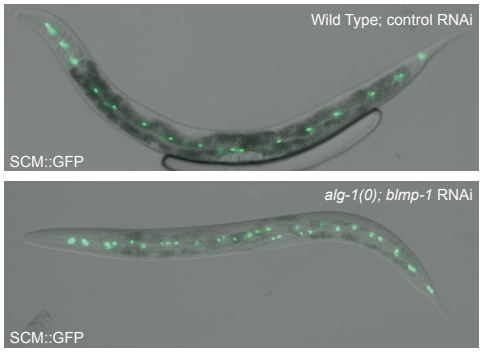

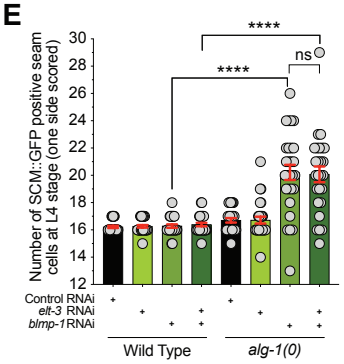

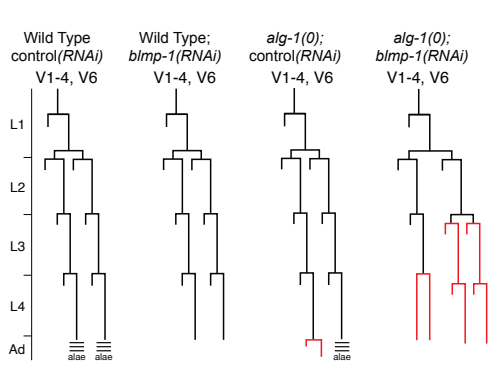

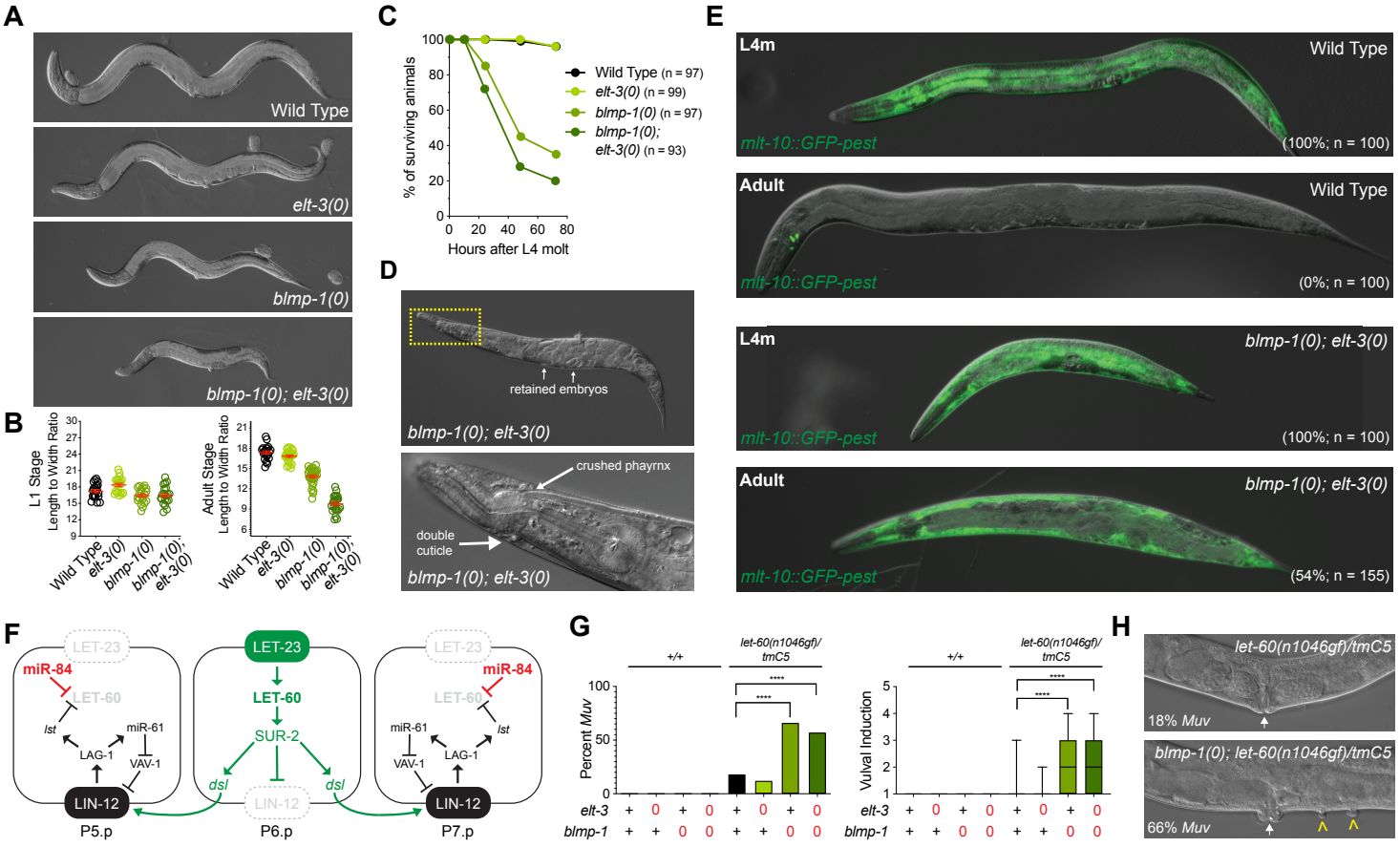
A
Wild Type
elt-3(0)
blmp-1(0)
blmp-1(0); elt-3(0)
B
L1 Stage
Length to Width Ratio
Adult Stage
Length to Width Ratio
Wild Type
elt-3(0)
blmp-1(0)
blmp-1(0); elt-3(0)
C
% of surviving animals
Hours after L4 molt
Wild Type (n = 97)
elt-3(0) (n = 99)
blmp-1(0) (n = 97)
blmp-1(0); elt-3(0) (n = 93)
D
retained embryos
blmp-1(0); elt-3(0)
crushed phayrnx
double cuticle
blmp-1(0); elt-3(0)
E
L4m
Wild Type
mlt-10::GFP-pest
(100%; n = 100)
Adult
Wild Type
mlt-10::GFP-pest
(0%; n = 100)
L4m
blmp-1(0); elt-3(0)
mlt-10::GFP-pest
(100%; n = 100)
Adult
blmp-1(0); elt-3(0)
mlt-10::GFP-pest
(54%; n = 155)
F
LET-23
miR-84
LET-60
lst
miR-61
LAG-1
VAV-1
LIN-12
P5.p
LET-23
LET-60
SUR-2
dsl
dsl
LIN-12
P6.p
LET-23
miR-84
LET-60
miR-61
lst
VAV-1
LAG-1
LIN-12
P7.p
G
+/+
let-60(n1046gf)/ tmC5
Percent Muv
Vulval Induction
elt-3
blmp-1
H
let-60(n1046gf)/tmC5
18% Muv
blmp-1(0); let-60(n1046gf)/tmC5
66% Muv

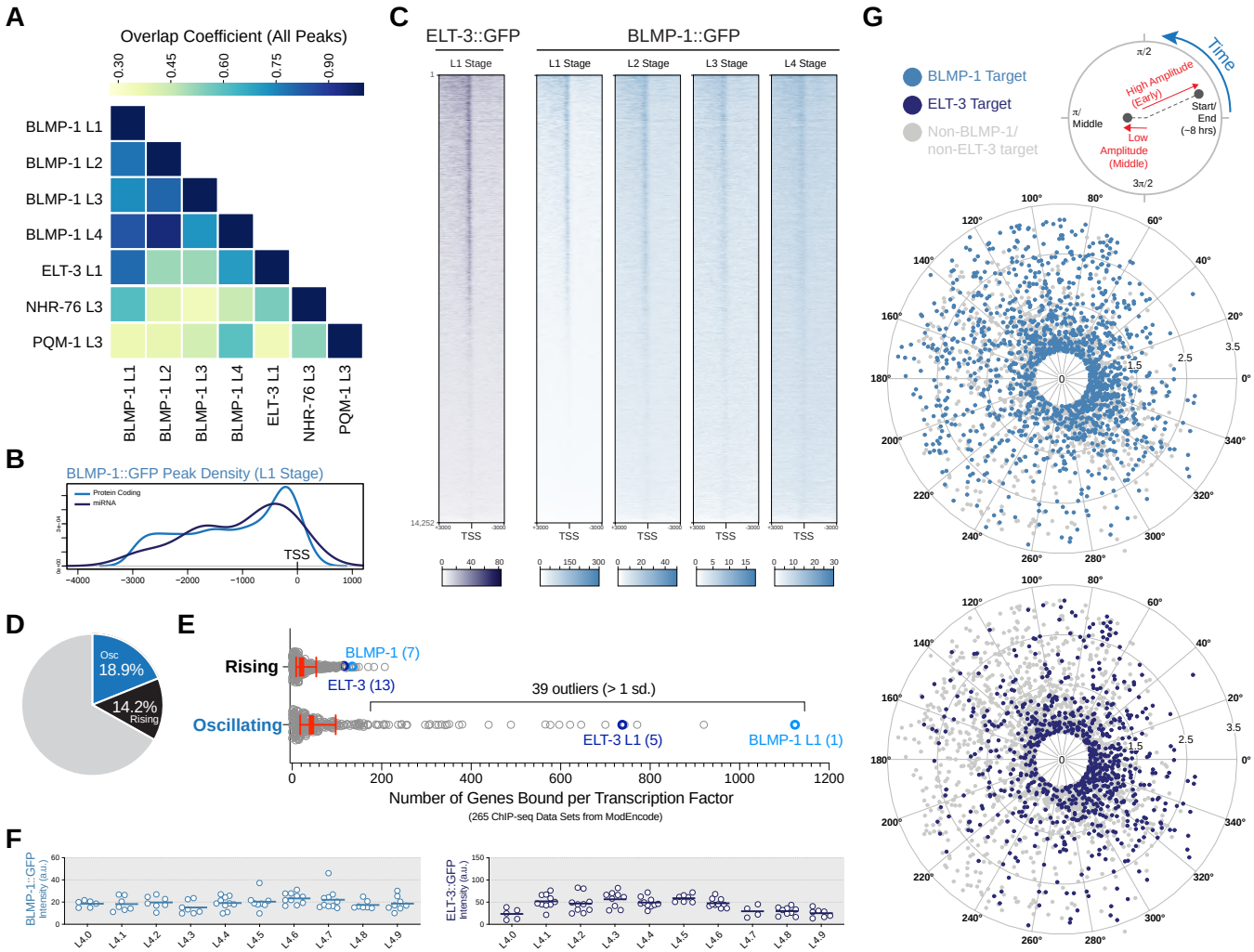
A
Overlap Coefficient (All Peaks)
0.30
0.45
0.60
0.75
0.90
BLMP-1 L1
BLMP-1 L2
BLMP-1 L3
BLMP-1 L4
ELT-3 L1
NHR-76 L3
PQM-1 L3
B
BLMP-1::GFP Peak Density (L1 Stage)
Protein Coding
miRNA
TSS
C
ELT-3::GFP
BLMP-1::GFP
L1 Stage
L2 Stage
L3 Stage
L4 Stage
TSS
D
Osc
18.9%
14.2%
Rising
E
Rising
Oscillating
BLMP-1 (7)
ELT-3 (13)
39 outliers (> 1 sd.)
ELT-3 L1 (5)
BLMP-1 L1 (1)
Number of Genes Bound per Transcription Factor
(265 ChIP-seq Data Sets from ModEncode)
F
BLMP-1::GFP Intensity (a.u.)
ELT-3::GFP Intensity (a.u.)
L4.0
L4.1
L4.2
L4.3
L4.4
L4.5
L4.6
L4.7
L4.8
L4.9
G
BLMP-1 Target
ELT-3 Target
Non-BLMP-1/
non-ELT-3 target
Time
High Amplitude
(Early)
Start/
End
(~8 hrs)
Low
Amplitude
(Middle)
Middle

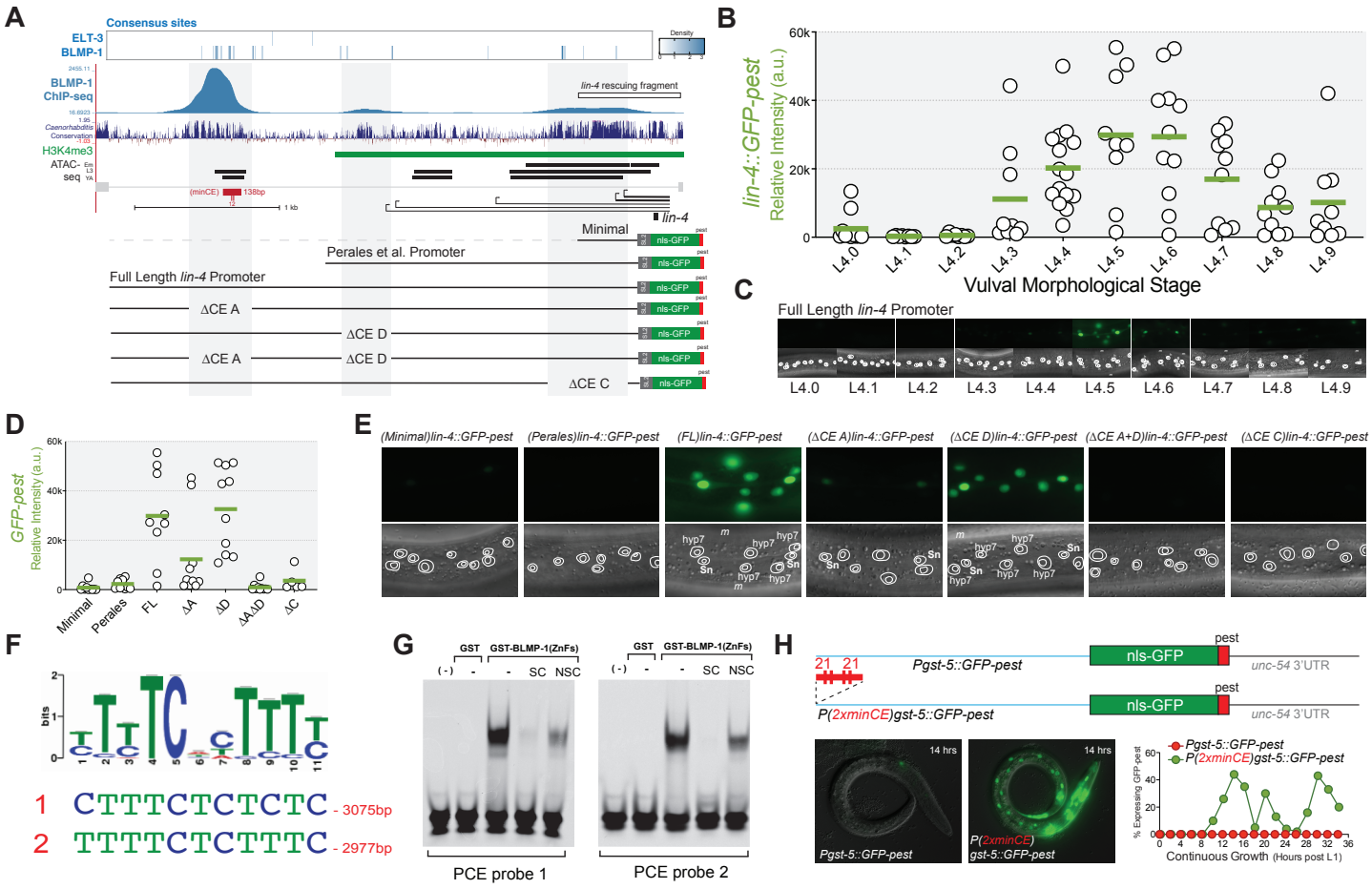
A
Consensus sites
ELT-3
BLMP-1
BLMP-1 ChIP-seq
lin-4 rescuing fragment
H3K4me3
ATAC-seq
(minCE) 138bp
1 kb
lin-4
Minimal
Perales et al. Promoter
Full Length lin-4 Promoter
ΔCE A
ΔCE D
ΔCE A
ΔCE D
ΔCE C
nls-GFP
pest
B
lin-4::GFP-pest
Relative Intensity (a.u.)
60k
40k
20k
0
L4.0
L4.1
L4.2
L4.3
L4.4
L4.5
L4.6
L4.7
L4.8
L4.9
Vulval Morphological Stage
C
Full Length lin-4 Promoter
L4.0
L4.1
L4.2
L4.3
L4.4
L4.5
L4.6
L4.7
L4.8
L4.9
D
GFP-pest
Relative Intensity (a.u.)
60k
40k
20k
0
Minimal
Perales
FL
ΔA
ΔD
ΔAΔD
ΔC
E
(Minimal)lin-4::GFP-pest
(Perales)lin-4::GFP-pest
(FL)lin-4::GFP-pest
(ΔCE A)lin-4::GFP-pest
(ΔCE D)lin-4::GFP-pest
(ΔCE A+D)lin-4::GFP-pest
(ΔCE C)lin-4::GFP-pest
hyp7
m
Sn
F
bits
2
1
0
1 CTTTCTCTCTC - 3075bp
2 TTTTCTCTTTC - 2977bp
G
GST
GST-BLMP-1(ZnFs)
(-)
-
-
SC
NSC
PCE probe 1
PCE probe 2
H
21
21
Pgst-5::GFP-pest
P(2xminCE)gst-5::GFP-pest
nls-GFP
pest
unc-54 3'UTR
14 hrs
Pgst-5::GFP-pest
P(2xminCE)
gst-5::GFP-pest
% Expressing GFP-pest
60
40
20
0
0
4
8
12
16
20
24
28
32
36
Continuous Growth (Hours post L1)

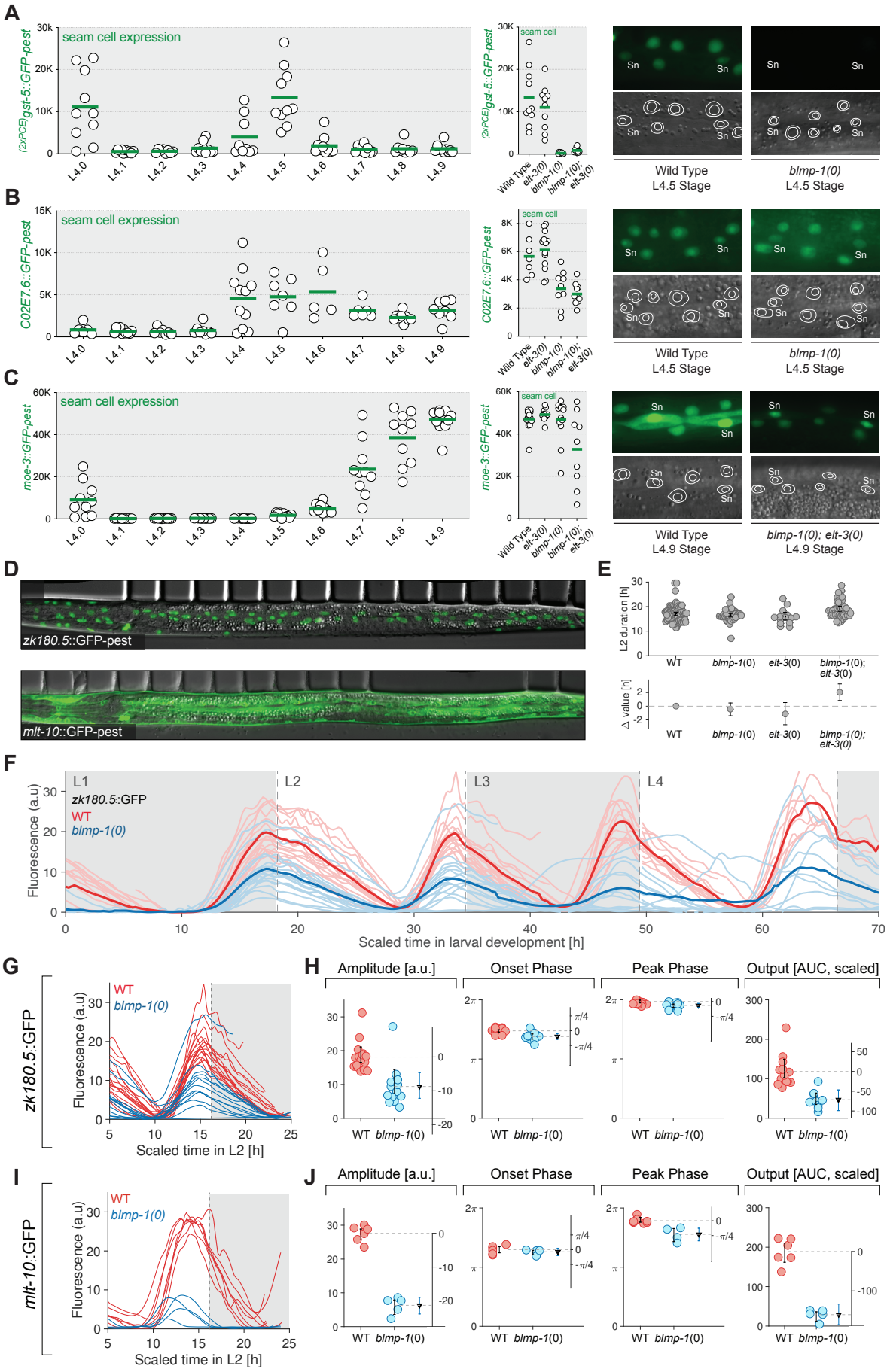
A
seam cell expression
(2xPCE)gst-5::GFP-pest
L4.0
L4.1
L4.2
L4.3
L4.4
L4.5
L4.6
L4.7
L4.8
L4.9
seam cell
Wild Type
elt-3(0)
blmp-1(0)
blmp-1(0); elt-3(0)
Sn
Wild Type
L4.5 Stage
blmp-1(0)
L4.5 Stage
B
C02E7.6::GFP-pest
C
moe-3::GFP-pest
Wild Type
L4.9 Stage
blmp-1(0); elt-3(0)
L4.9 Stage
D
zk180.5::GFP-pest
mlt-10::GFP-pest
E
L2 duration [h]
Δ value [h]
WT
blmp-1(0)
elt-3(0)
blmp-1(0); elt-3(0)
F
L1
L2
L3
L4
zk180.5:GFP
WT
blmp-1(0)
Fluorescence (a.u)
Scaled time in larval development [h]
G
zk180.5:GFP
Scaled time in L2 [h]
H
Amplitude [a.u.]
Onset Phase
Peak Phase
Output [AUC, scaled]
I
mlt-10:GFP
J

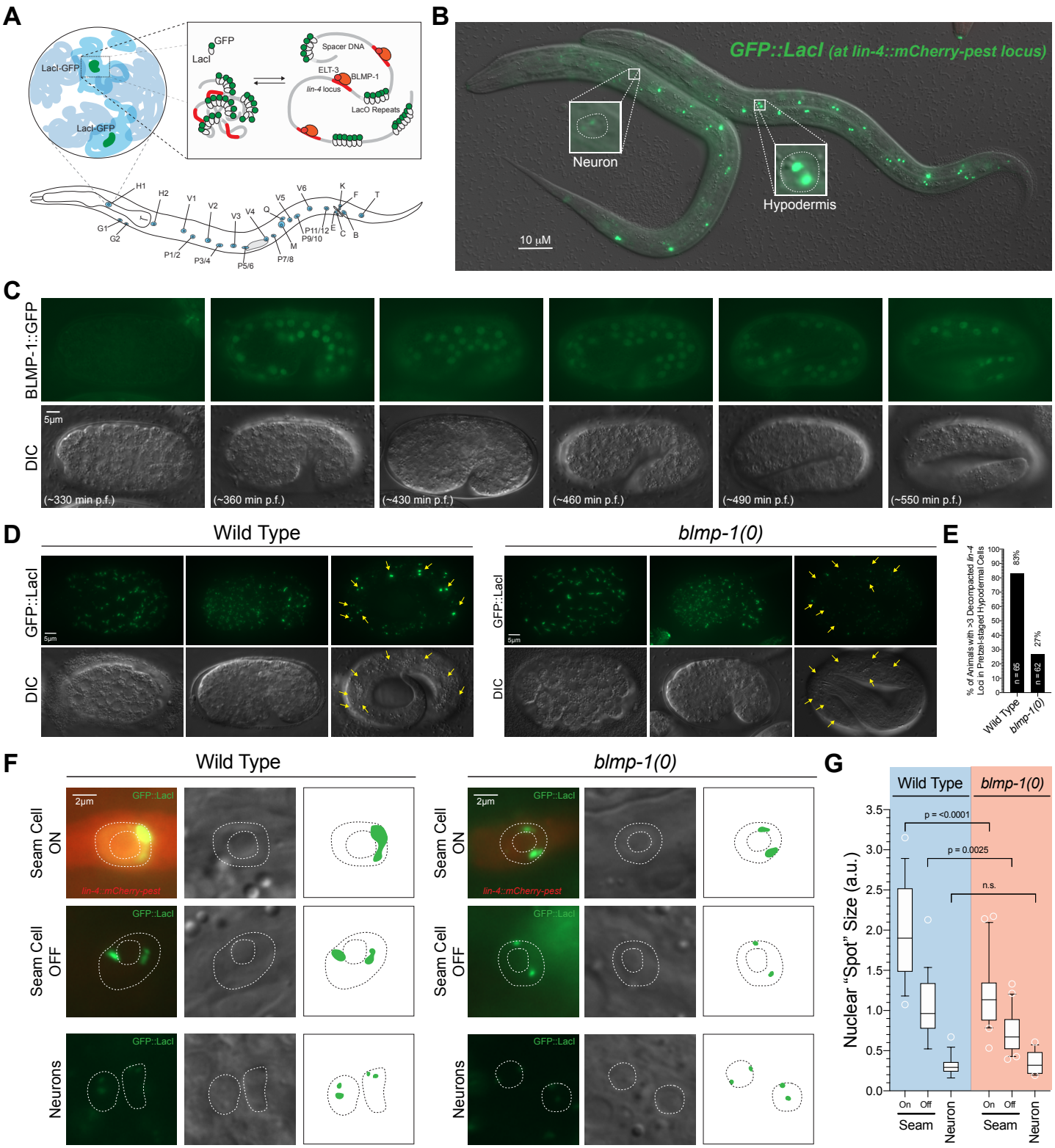
A
LacI-GFP
LacI-GFP
GFP
LacI
Spacer DNA
ELT-3
BLMP-1
lin-4 locus
LacO Repeats
H1
H2
V1
V2
V3
V4
V5
V6
K
F
T
Q
G1
G2
P1/2
P3/4
P5/6
P7/8
M
P11/12
P9/10
E
C
B
B
GFP::LacI (at lin-4::mCherry-pest locus)
Neuron
Hypodermis
10 μM
C
BLMP-1::GFP
DIC
5μm
(~330 min p.f.)
(~360 min p.f.)
(~430 min p.f.)
(~460 min p.f.)
(~490 min p.f.)
(~550 min p.f.)
D
Wild Type
blmp-1(0)
GFP::LacI
DIC
5μm
E
% of Animals with >3 Decompacted lin-4 LocI in Pretzel-staged Hypodermal Cells
83%
27%
n = 65
n = 62
Wild Type
blmp-1(0)
F
Wild Type
blmp-1(0)
Seam Cell ON
Seam Cell OFF
Neurons
2μm
GFP::LacI
lin-4::mCherry-pest
G
Wild Type
blmp-1(0)
Nuclear "Spot" Size (a.u.)
p = <0.0001
p = 0.0025
n.s.
On
Off
Seam
Neuron

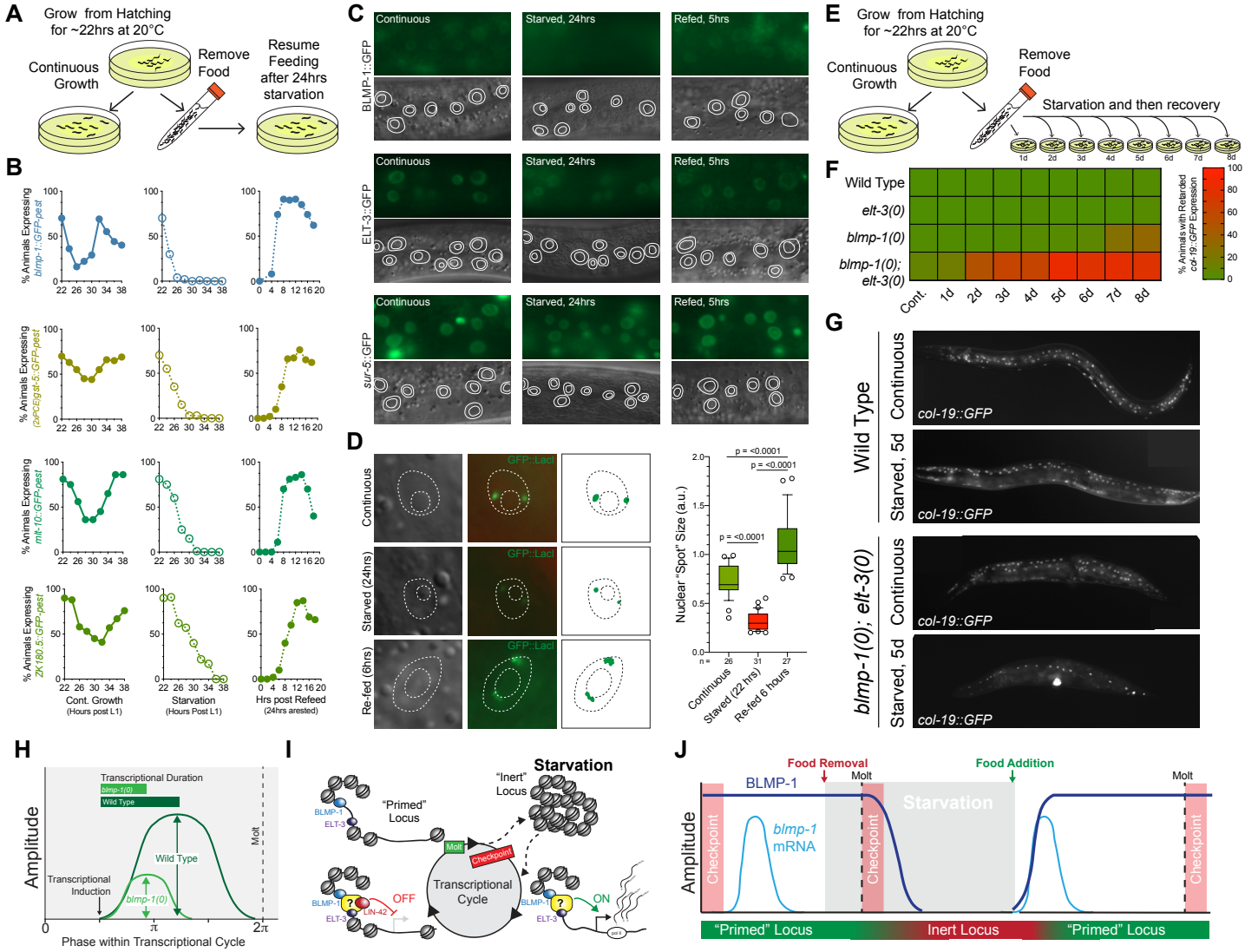
A
Grow from Hatching for ~22hrs at 20°C
Continuous Growth
Remove Food
Resume Feeding after 24hrs starvation
B
% Animals Expressing blmp-1::GFP-pest
% Animals Expressing (2xPCE)gst-5::GFP-pest
% Animals Expressing mlt-10::GFP-pest
% Animals Expressing ZK180.5::GFP-pest
Cont. Growth (Hours post L1)
Starvation (Hours Post L1)
Hrs post Refeed (24hrs arested)
C
Continuous
Starved, 24hrs
Refed, 5hrs
BLMP-1::GFP
ELT-3::GFP
sur-5::GFP
D
Continuous
Starved (24hrs)
Re-fed (6hrs)
GFP::LacI
Nuclear "Spot" Size (a.u.)
p = <0.0001
Continuous
Starved (22 hrs)
Re-fed 6 hours
E
Grow from Hatching for ~22hrs at 20°C
Continuous Growth
Remove Food
Starvation and then recovery
F
Wild Type
elt-3(0)
blmp-1(0)
blmp-1(0); elt-3(0)
Cont.
% Animals with Retarded col-19::GFP Expression
G
Wild Type
blmp-1(0); elt-3(0)
Continuous
Starved, 5d
col-19::GFP
H
Transcriptional Duration
blmp-1(0)
Wild Type
Amplitude
Transcriptional Induction
Molt
Phase within Transcriptional Cycle
I
Starvation
"Primed" Locus
"Inert" Locus
Molt
Checkpoint
Transcriptional Cycle
OFF
ON
LIN-42
J
Food Removal
Food Addition
BLMP-1
Molt
Starvation
blmp-1 mRNA
Amplitude
Checkpoint
"Primed" Locus
Inert Locus

Transcription Dynamics

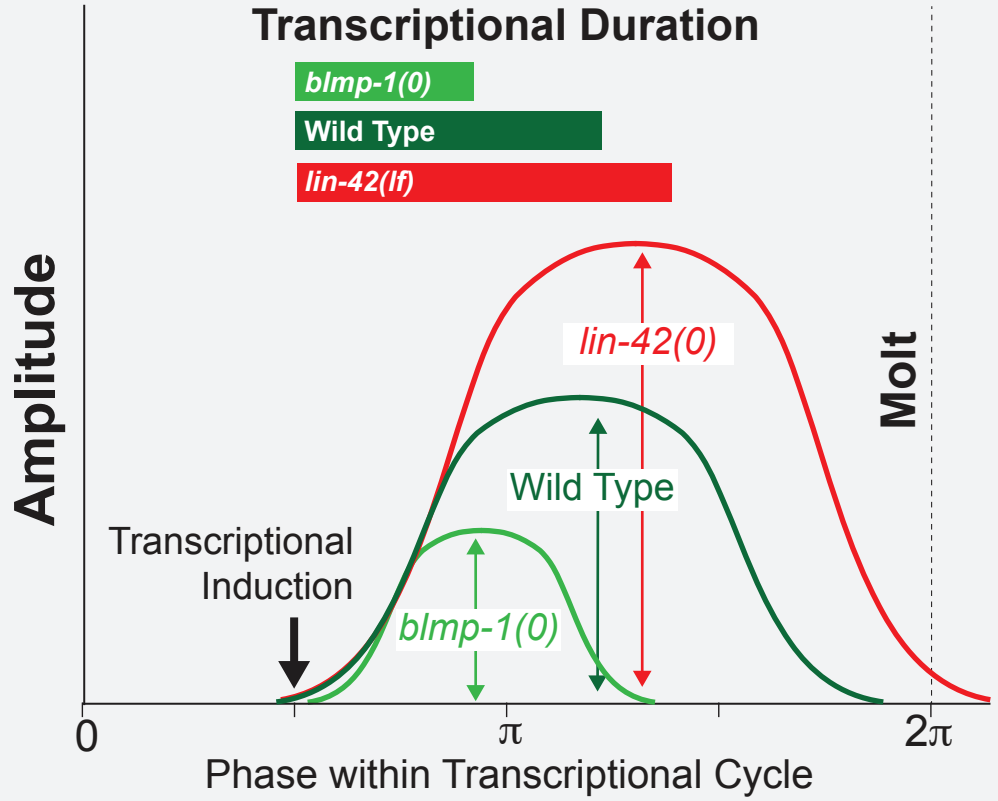

BLMP-1 priming mechanism